JGP Journal of General Physiology

ARTICLE

Hippocampal neurons maintain a large PtdIns(4)*P* pool that results in faster PtdIns(4,5)P_2 synthesis

Lizbeth de la Cruz[1], Christopher Kushmerick[2], Jane M. Sullivan[1], Martin Kruse[3], and Oscar Vivas[1]

PtdIns(4,5)P_2 is a signaling lipid central to the regulation of multiple cellular functions. It remains unknown how PtdIns(4,5)P_2 fulfills various functions in different cell types, such as regulating neuronal excitability, synaptic release, and astrocytic function. Here, we compared the dynamics of PtdIns(4,5)P_2 synthesis in hippocampal neurons and astrocytes with the kidney-derived tsA201 cell line. The experimental approach was to (1) measure the abundance and rate of PtdIns(4,5)P_2 synthesis and precursors using specific biosensors, (2) measure the levels of PtdIns(4,5)P_2 and its precursors using mass spectrometry, and (3) use a mathematical model to compare the metabolism of PtdIns(4,5)P_2 in cell types with different proportions of phosphoinositides. The rate of PtdIns(4,5)P_2 resynthesis in hippocampal neurons after depletion by cholinergic or glutamatergic stimulation was three times faster than for tsA201 cells. In tsA201 cells, resynthesis of PtdIns(4,5)P_2 was dependent on the enzyme PI4K. In contrast, in hippocampal neurons, the resynthesis rate of PtdIns(4,5)P_2 was insensitive to the inhibition of PI4K, indicating that it does not require de novo synthesis of the precursor PtdIns(4)*P*. Measurement of phosphoinositide abundance indicated a larger pool of PtdIns(4)*P*, suggesting that hippocampal neurons maintain sufficient precursor to restore PtdIns(4,5)P_2 levels. Quantitative modeling indicates that the measured differences in PtdIns(4)*P* pool size and higher activity of PI4K can account for the experimental findings and indicates that high PI4K activity prevents depletion of PtdIns(4)*P*. We further show that the resynthesis of PtdIns(4,5)P_2 is faster in neurons than astrocytes, providing context to the relevance of cell type–specific mechanisms to sustain PtdIns(4,5)P_2 levels.

Introduction

Modulation of neuronal firing frequency relies on the regulation of ion channel activities. Substantial evidence in the last two decades puts phosphatidylinositol 4,5-bisphosphate (PtdIns(4,5)P_2) as a critical controller of ion channels (Hille et al., 2015) and, therefore, as a potential regulator of neuronal excitability and firing patterns. Many of these studies relied on the expression of ion channels in heterologous expression systems where the levels of PtdIns(4,5)P_2 were easily manipulated. Less work has been done using neurons. Work in neurons and neuron-derived immortalized cell lines emphasizes the relevance of PtdIns(4,5)P_2 for the proper function of neurons by assessing chronic depletion or addition of PtdIns(4,5)P_2 (Hackelberg and Oliver, 2018; Raghu et al., 2019; Rohács et al., 2005; Willars et al., 1998; Winks et al., 2005). In our work, we focused on the rate of resynthesis after short-term depletion by G-protein coupled receptor (GPCR) activation.

Previously, we showed that sympathetic neurons, peripheral neurons, resynthesize PtdIns(4,5)P_2 faster than tsA201 cells that are derived from the human embryonic kidney immortalized cell line. The underlying mechanism in peripheral neurons was suggested to be an increase in PI4K activity following PtdIns(4,5)P_2 depletion, but, interestingly, the relative amount of phosphatidylinositol (PtdIns), phosphatidylinositol 4-phosphate (PtdIns(4)*P*), and PtdIns(4,5)P_2 in sympathetic neurons were the same as in tsA201 cells (Kruse et al., 2016). Now, we wanted to test whether the fast recovery of PtdIns(4,5)P_2 observed in peripheral neurons is conserved in neurons from the central nervous system and in glial cells. We are also interested in understanding how differences in phosphoinositide metabolism contribute to functional differences between cell types. Differences in dynamics of PtdIns(4,5)P_2 resynthesis in different cell types, especially between neurons and glia, would introduce a new perspective on the roles of PtdIns(4,5)P_2 in the brain.

PtdIns(4,5)P_2 comprises only 2% of total phosphoinositides (Traynor-Kaplan et al., 2017; Willars et al., 1998; Xu and Loew, 2003) and localizes mainly at the plasma membrane (PM) where it interacts with ion channels and other signaling proteins. Its synthesis involves sequential phosphorylation of PtdIns and

[1]Department of Physiology and Biophysics, University of Washington, Seattle, WA; [2]Department of Physiology and Biophysics, Universidade Federal de Minas Gerais, Belo Horizonte, Brazil; [3]Department of Biology and Program in Neuroscience, Bates College, Lewiston, ME.

Correspondence to Oscar Vivas: vivas@uw.edu; Martin Kruse: mkruse@bates.edu.

© 2022 De La Cruz et al. This article is distributed under the terms of an Attribution–Noncommercial–Share Alike–No Mirror Sites license for the first six months after the publication date (see http://www.rupress.org/terms/). After six months it is available under a Creative Commons License (Attribution–Noncommercial–Share Alike 4.0 International license, as described at https://creativecommons.org/licenses/by-nc-sa/4.0/).

PtdIns(4)*P* on the inositol headgroup in positions 4 and 5. Synthesis of PtdIns(4,5)P_2 from other sources such as the phosphorylation of PtdIns(5)*P* or dephosphorylation of PtdIns(3,4,5)P_3 is relatively minor. Some mathematical models of this metabolism depict the reaction steps in two dimensions, occurring only at the PM (Falkenburger et al., 2010; Olivença et al., 2018). However, PtdIns and PtdIns(4)*P* are abundant in other internal membranes such as the endoplasmic reticulum and Golgi (Hammond et al., 2014; Pemberton et al., 2020; Várnai et al., 2017; Zewe et al., 2020); hence, understanding the abundance and distribution of all phosphoinositide species in internal membranes is an essential step to model PtdIns(4,5)P_2 metabolism. The development of biosensors for PtdIns(4)*P* and PtdIns has brought us closer to this goal.

The phosphorylation steps are counterbalanced by dephosphorylation reactions mediated by lipid phosphatases that remove phosphate groups in the 5 and 4 positions of the inositol ring. The rate of PtdIns(4,5)P_2 synthesis is then controlled by the balance of phosphorylation and dephosphorylation and the concentration of substrates.

Two techniques are ideal to follow changes in PtdIns(4,5)P_2 levels, labeling with sensors and mass spectrometry. Genetically encoded sensors exploit PtdIns(4,5)P_2-binding domains tagged with fluorescent proteins. The most important characteristic of this tool is its ability to follow changes in real time. Two commonly used sensors are $PH_{PLC\delta1}$ and Tubby (R322H; Quinn et al., 2008; Stauffer et al., 1998; Szentpetery et al., 2009; Várnai and Balla, 1998). We have previously shown that both sensors report the same dynamics of PtdIns(4,5)P_2 in the kidney-derived tsA201 cell line and in neurons (Kruse et al., 2016). On the other hand, mass spectrometry allows quantitative comparison of the abundance of PtdIns(4,5)P_2 relative to PtdIns and PtdIns(4)*P* (Traynor-Kaplan et al., 2017) across cell types or treatment conditions.

In this work, we determined the rate of PtdIns(4,5)P_2 synthesis using $PH_{PLC\delta1}$, assessed the levels of phosphoinositides using mass spectrometry, and combined the data with a mathematical model to understand the mechanism that allows hippocampal neurons to resynthesize PtdIns(4,5)P_2 quickly—sustaining high levels of the precursor PtdIns(4)*P*.

Materials and methods

Reagents

L-glutamate, oxotremorine methiodide (oxo-M), GSK-A1, sodium formate, HCl, and trimethylsilyl-diazomethane (2.0 M in diethyl ether or hexanes) were from Sigma-Aldrich. Mass spectrometry-grade methanol, chloroform, dichloromethane, and acetonitrile were from Thermo Fisher Scientific.

Cells

Human embryonic kidney cell line

The tsA201 cell line (RRID: CVCL_2737; Sigma-Aldrich), derived from human embryonic kidney cells, was cultured in DMEM (Gibco) supplemented with 10% FBS (Sigma-Aldrich) and 2% penicillin/streptomycin in 5% CO_2 at 37°C. Cells were transfected at ∼75% confluency with Lipofectamine 3000 and plated on poly-L-lysine–coated glass chips (Thomas Scientific).

Hippocampal neurons and cortical astrocytes

Animals were handled according to guidelines of the University of Washington Institutional Animal Care and Use Committee. Hippocampal neurons and cortical astrocytes were isolated from neonatal mice (Pratt et al., 2011) and rats (Brewer et al., 1993) of both sexes and incubated in 5% CO_2 at 37°C. Hippocampal neurons were cultured under two different medium conditions: (1) MEM supplemented with GlutaMAX (1%), B27, sodium pyruvate, horse serum (10%), 25 mM HEPES, and 20 mM glucose or (2) Neurobasal medium supplemented with GlutaMAX (1%) and B27. Astrocytes were cultured in MEM supplemented with GlutaMAX (1% V/V), 5% FCS, and 20 mM glucose. Penicillin/streptomycin (0.1%) was added to the culture medium. We note that we are unaware of the effects of the different media compositions on the lipid content of the cell types evaluated. Notably, neurons cultured in both medium conditions gave similar results. Hippocampal neurons were transfected after 12–15 d with Lipofectamine 2000 using Opti-MEM and used for experiments 24–48 h after transfection. Transfection efficiency was 5–10%. Astrocytes were transfected after 7 d with Lipofectamine 2000 using Opti-MEM and used for experiments 24 h after transfection. Transfection efficiency was ∼40%. Fast PtdIns(4,5)P_2 metabolism was observed in both mouse and rat hippocampal neurons without significant differences. Hippocampal neurons from mice were used for FAPP1 and BcPI-PLC (ANH) expression while other experiments were developed in hippocampal neurons from rats.

Plasmids

Human pleckstrin homology (PH) domain probes $PH_{PLC\delta1}$-ECFP and PH $PH_{PLC\delta1}$-EYFP plasmids were provided by Kees Jalink, the Netherlands Cancer Institute (Amsterdam, Netherlands); P4M-YFP and BcPI-PLC(ANH)-GFP from Tamas Balla, National Institutes of Health (Bethesda, MD); mCherry-P4M and FAPP1-GFP from Gerald Hammond, University of Pittsburgh (Pittsburgh, PA); and untagged M_1 receptor (M_1R) from Neil M. Nathanson, University of Washington.

Confocal microscopy

Hippocampal neurons, astrocytes, and tsA201 cells were imaged in Ringer's solution 24 h after transfection. Ringer's solution contained 150 mM NaCl, 2.5 mM KCl, 2 mM $CaCl_2$, 1 mM $MgCl_2$, 10 mM HEPES, and 8 mM glucose, adjusted with NaOH to pH 7.4. All agonists were applied for 20–50 s. Agonists were dissolved in Ringer's solution to obtain a final concentration of 10 µM oxo-M or 1 mM L-Glutamic acid (L-Glu). The bath perfusion system was controlled to 1–2 ml/min. Fluorophores were excited with an argon laser for CFP and YFP (458 and 514 nm) and a helium/neon laser for mCherry (594 nm), and emission was monitored using a Plan-Apochromat 40×/1.40 oil DIC M27 objective (confocal, LSM 710; Zeiss). Confocal images for Figs. 3, E and L; 4, A, C, and E; and 7, B, F, and G were obtained with a high-resolution AiryScan system (Zeiss LSM 880) run by ZEN black v2.3. A Plan-Apochromat 63×/1.40 NA oil immersion objective was used. Fluorescent proteins were excited with a 405 nm diode, 458–514 nm argon, and 561 nm laser. Emission light was detected using an Airyscan 32 GaAsP

detector and appropriate emission filter sets. The point spread functions were calculated using ZEN black software using 0.1 µm fluorescent microspheres. After deconvolution, the point spread functions were 124 nm in x–y and 216 nm in z (488 nm excitation) and 168 nm in x–y and 212 nm in z (594 nm excitation). The temperature inside the microscope housing was 27–30°C. Time series were taken with an interval of 2–10 s.

Lipid extraction and mass spectrometry

The mass spectrometry method was modified from Traynor-Kaplan et al. (2017). Each lipid determination for mass spectrometry was conducted from a 35 mm ∼70% confluent dish of tsA201 cells or from both sides of the hippocampal area from newborn (P1) male rats. tsA201 cells were washed twice with Ringer's solution and resuspended with a scraper in ice-cold methanol/1 N HCl solution. Hippocampi were minced in ice to prevent PtdIns(4,5)P_2 depletion during the extraction, as previously shown (Hille et al., 2015; Kruse et al., 2016). Tissue was pelleted by centrifugation at 20,000 *g* for 3 min at 4°C. Pellets were resuspended in ice-cold water. Then, 10 µl of 6 N HCl, 100 µl of N-butanol, and internal standards (150 ng of 37:4 PtdIns and 20 ng of 37:4 PtdIns(4)*P* and 37:4 PtdIns(4,5)P_2; Avanti Polar Lipids) were added to each sample. Samples were vortexed vigorously for 1 min and allowed to sit on ice for 10 min. After that, samples were centrifuged at 20,000 *g* for 3 min at 4°C. The N-butanol phase was transferred to a new tube and a second N-butanol extraction step was conducted. Then, three chloroform extractions followed the addition of 100 µl of chloroform to each sample. Samples were vigorously vortexed and centrifuged at 20,000 *g* for 3 min at 4°C. The chloroform phases were combined with the N-butanol extraction. Finally, the butanol/chloroform extract was centrifuged and the water phase was discarded.

The butanol/chloroform-extracted lipid samples were dried under N_2 (Biotage TM evaporator) and resuspended in 90 µl of methanol/CH_2Cl_2. 20 µl of 2 M trimethylsilyl-diazomethane was added to each sample, and the samples were incubated for 1 h before the measurement. Quantification was performed on an ultraperformance liquid chromatography (UPLC) coupled Xevo TQ-S triple quadrupole mass spectrometer (Waters Corp). Peak areas of individual lipid species were quantified using QuanLynx TM software, and peak areas were normalized to the internal standards.

On an important note, we are comparing the phosphoinositide content in P1 hippocampi measured by mass spectrometry with the imaging from neurons obtained at P1 and cultured for up to 15 d (DIV 15). We have assumed that PtdIns(4,5)P_2 metabolism is identical in hippocampal neurons at P1 and DIV15. Whether PtdIns(4,5)P_2 metabolism differs as cells are cultured or during development will need further testing. Additionally, lipids extracted from the hippocampus reflect the lipids in different cell types including, but not limited to, neurons and astrocytes.

Mathematical modeling

Mathematical modeling was performed using the programming language R version 3.6.3 (R Project for Statistical Computing, RRID: SCR_001905). Differential equations were solved in R using the library "deSolve" version 1.28.0 and graphical analysis was performed by generating plots with the library "ggplot2" version 3.3. Initial estimates for parameters were based on a previously published model for phosphoinositide metabolism in tsA201 cells (Falkenburger et al., 2010).

Experimental design and statistical analyses

Confocal images were analyzed with Fiji (Schindelin et al., 2012). Photobleaching was corrected in some time series, using the analysis tool "Bleach correction" with an exponential fit. We measured the changes in the fluorescence intensity from a region of interest drawn in the cytosol, excluding the PM and the nucleus. For both $PH_{PLC\delta1}$ and P4M, the cytosolic intensity values were normalized to the first point and the y axis was inverted. Here, we assumed that the kinetics of the fluorescence changes in the cytosol mirror the kinetics in the PM, but inverted (Fig. S1). We fitted a single exponential during washout and interpreted it as the rate of PtdIns(4,5)P_2 resynthesis. Because the PtdIns(4,5)P_2 resynthesis showed a significant delay in astrocytes, we also determinate the half-time recovery.

For data analysis, IGOR Pro and GraphPad Prism version 8.0 (GraphPad Software) were used. We estimated the number of cells required for each experimental series to determine an effect size of 50% relative to the control group, with an 80% statistical power and a 95% confidence level. The number of cells was collected from at least two independent experiments. Calculations accounted for each technique's variability, and this variability was measured from previously reported experiments from our laboratory. Statistics in text and error bars in figures are given as mean ± SEM. Student's *t* test (two tails, independent) was used to test for statistical significance. Exact P values are reported in figures and text.

Online supplemental material

Fig. S1 shows the kinetics of $PH_{PLC\delta1}$ translocation measured in the cytosol mirror kinetics in the PM. Table S1 provides details of the parameters used in the new model for hippocampal neurons.

Results

Resynthesis of PtdIns(4,5)P_2 in hippocampal neurons is rapid

Previously, we showed that peripheral sympathetic neurons recover rapidly from receptor-induced depletion of PtdIns(4,5)P_2. We want to test whether this property is also encountered in central neurons. We studied the rate of PtdIns(4,5)P_2 resynthesis in hippocampal neurons. Fig. 1 A illustrates the experimental approach: the fluorescence of a PtdIns(4,5)P_2 biosensor ($PH_{PLC\delta1}$) is used as a readout of PtdIns(4,5)P_2 levels. Before any stimulation, the localization of the biosensor is biased toward the PM. During the stimulation, the biosensor moves to the cytosol, as the inositol ring of PtdIns(4,5)P_2 is cleaved off, producing Ins(1,4,5)P_3 and diacylglycerol. Once the agonist is removed, the biosensor gradually returns to the PM. This recovery phase corresponds to the resynthesis of PtdIns(4,5)P_2. Using this protocol, we followed the biosensor relocalization rate during washout and interpreted it as the rate of PtdIns(4,5)P_2 resynthesis.

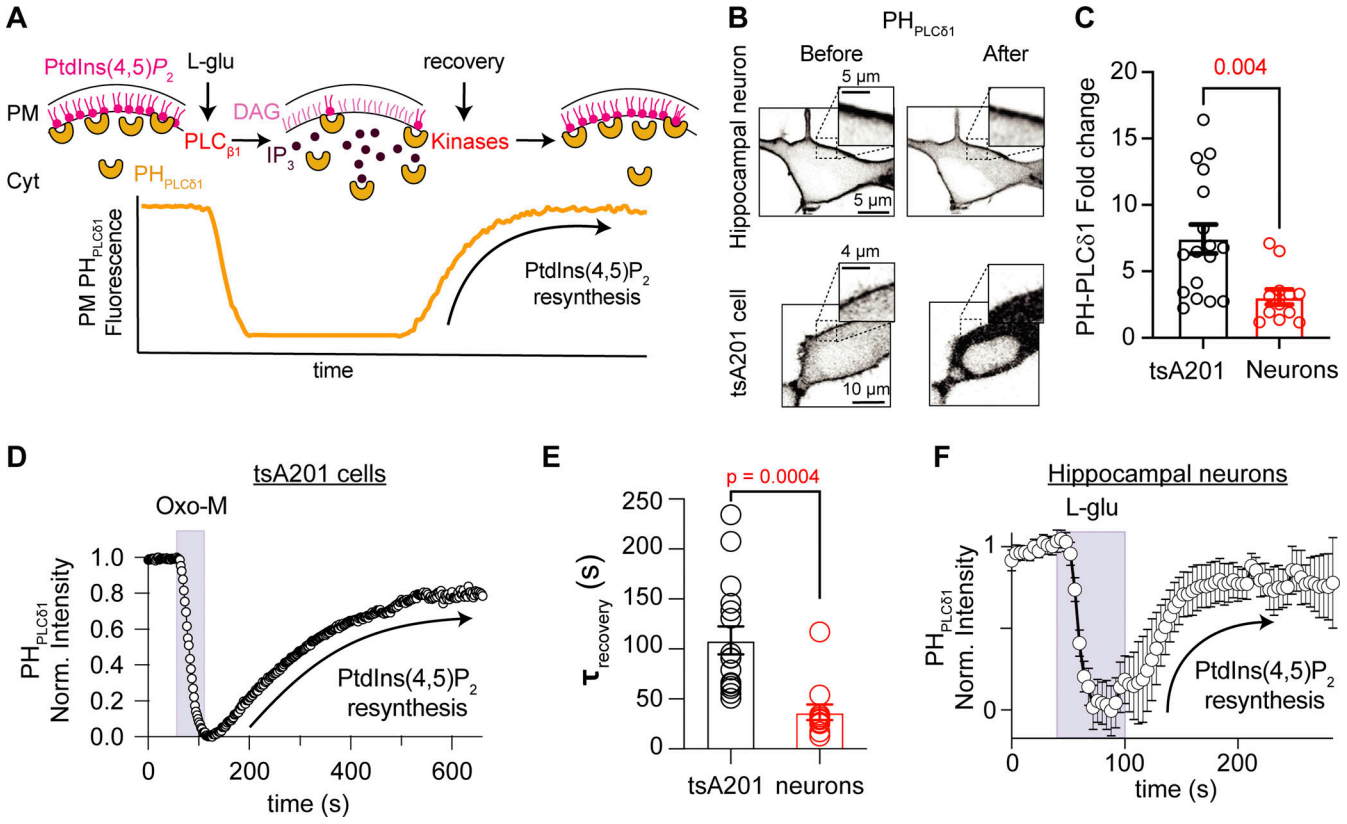

Figure 1. **Resynthesis of PtdIns(4,5)P_2 in hippocampal neurons is rapid. (A)** Schematic representation of the experimental approach. $PH_{PLC\delta1}$ sensors bind to PtdIns(4,5)P_2 at the PM. The sensor translocates to the cytosol after PtdIns(4,5)P_2 depletion. Resynthesis of PtdIns(4,5)P_2 after washout returns $PH_{PLC\delta1}$ sensors at the PM. **(B)** Representative confocal images of $PH_{PLC\delta1}$ fluorescence (inverted contrast) before and during receptor stimulation of an isolated hippocampal neuron and a tsA201 cell overexpressing M_1R. Enlarged inserts are shown in the upper part of each image. **(C)** $PH_{PLC\delta1}$ fold change in cytosol during stimulation. **(D)** Representative time course of inverted normalized cytosolic intensity of $PH_{PLC\delta1}$ in a tsA201 cell before, during, and after 10 µM oxo-M. **(E)** Comparison of the exponential time constant of recovery as a proxy for PtdIns(4,5)P_2 resynthesis in hippocampal neurons (n = 12) and tsA201 cells (n = 16). **(F)** Average time course of inverted normalized cytosolic intensity of $PH_{PLC\delta1}$ in isolated hippocampal neurons before, during, and after 1 mM L-Glu.

Isolated hippocampal neurons exhibited clear localization of $PH_{PLC\delta1}$ probes at the PM before stimulation. As expected, stimulation with glutamate induced biosensor translocation to the cytosol and a clear reduction of this sensor in the PM (Fig. 1 B). Not all $PH_{PLC\delta1}$ translocated into the cytoplasm upon glutamate receptor activation, as much of the $PH_{PLC\delta1}$ was retained at the PM in hippocampal neurons (Fig. 1, B and C), and the translocation to the cytosol was only 40% of that in tsA201 cells (fold change in neurons was 7.5 ± 1.1, n = 17; in tsA201 it was 3.1 ± 1.9, n = 12, P = 0.004, Fig. 1 C). Recall that although we measured the $PH_{PLC\delta1}$ biosensor fluorescence in the cytosol, our plots show traces that were normalized and inverted. The kinetics of the signal change measured at the PM or the cytosol are complementary and only differ in the direction (Fig. S1). Changes in the time course of the fluorescence intensity indicated PtdIns(4,5)P_2 hydrolysis during stimulation followed by recovery corresponding to the phase of PtdIns(4,5)P_2 resynthesis for tsA201 cells and hippocampal neurons (Fig. 1, D and F). The phase of resynthesis was fitted with a single exponential function with an average time constant of 109 ± 14 s (n = 16) in tsA201 cells (Fig. 1, D and E) and 36.7 ± 7.8 s (n = 12) in hippocampal neurons (Fig. 1, E and F). Thus, the rate of PtdIns(4,5)P_2 resynthesis in hippocampal neurons was three times faster.

Fast resynthesis does not depend on the stimulated receptor

A caveat to this comparison is that in tsA201 cells we activated overexpressed muscarinic acetylcholine receptor 1 (M_1R) rather than endogenous metabotropic glutamate receptors. Previously, we also activated endogenous M_1R to study the rate of PtdIns(4,5)P_2 resynthesis in sympathetic neurons (Kruse et al., 2016). Is it possible that the fast rate of PtdIns(4,5)P_2 resynthesis in hippocampal neurons is observed only after glutamate stimulation? While M_1 receptors are members of the Class A family of GPCRs, metabotropic glutamate receptors belong to the Class C family, having quite different structures (Kruse et al., 2014; Rosenbaum et al., 2009). These different structures might lead to differences in how the PLC signaling pathway is activated and terminated. Hippocampal neurons express glutamate and muscarinic receptors, and both receptors couple to $G_{\alpha q}$ proteins and activate PLC, causing PtdIns(4,5)P_2 depletion. We therefore compared the rate of PtdIns(4,5)P_2 resynthesis after stimulation of both glutamate and muscarinic receptors in the same neuron. In this set of experiments, hippocampal neurons expressing $PH_{PLC\delta1}$ were stimulated first with glutamate and then, after 10 min of washout, with a muscarinic agonist, oxo-M. The time course of $PH_{PLC\delta1}$ fluorescence intensity was similar for glutamate (Fig. 2, A and B) and oxo-M (Fig. 2, C and D). In these

experiments, the time constant of $PH_{PLC\delta1}$ recovery was 20.3 ± 3.5 s after glutamate and 25.6 ± 6.4 after oxo-M stimulation (Fig. 2 E, n = 6). The magnitude of $PH_{PLC\delta1}$ translocation was not different between agonists ($F/F_{0\text{-}L\text{-}Glu}$ = 1.7 ± 0.2, $F/F_{0\text{-}oxo\text{-}M}$ = 1.8 ± 0.1, P value = 0.5). Hence, the fast resynthesis of PtdIns(4,5)P_2 in hippocampal neurons does not depend on the specific $G_{\alpha q}$ proteincoupled receptor used to deplete PtdIns(4,5)P_2.

Additionally, we compared the kinetics of PtdIns(4,5)P_2 recovery upon oxo-M stimulation using a different sensor: $Tubby_C^{R332H}$. The main difference between $PH_{PLC\delta1}$ and $Tubby_C^{R332H}$ is that $Tubby_C^{R332H}$ cannot bind to inositol (1,4,5)-trisphosphate. The rate of recovery using $Tubby_C^{R332H}$ was similar to that using $PH_{PLC\delta1}$ (Fig. 2 F) with a time constant of 23.2 ± 4.2 s (Fig. 2 G, n = 5). These results support the idea that the fast resynthesis of PtdIns(4,5)P_2 in hippocampal neurons is independent of the sensor used and that the translocation of the biosensor is not caused by production of inositol (1,4,5)-trisphosphate, but by hydrolysis of PtdIns(4,5)P_2.

PtdIns(4)*P* is relatively more abundant in hippocampal neurons than tsA201 cells and it is resistant to depletion

Next, we asked how hippocampal neurons were able to sustain such high rates of resynthesizing PtdIns(4,5)P_2. An important clue came when we measured the relative abundance of PtdIns, PtdIns*P*, and PtdInsP_2 in the hippocampus and tsA201 cells by mass spectrometry. Of the total phosphoinositides, the percentages of these three lipids were 93.0 ± 0.5%, 2.8 ± 0.2%, and 4.2 ± 0.4%, respectively, in tsA201 cells (Fig. 3 A). Lipids from the hippocampal formation were extracted from P1 pups. In these hippocampal extracts, the percentages were 82.8 ± 5.6%, 15.8 ± 5.8%, and 1.3 ± 0.3% for PtdIns, PtdIns*P*, and PtdInsP_2, respectively (Fig. 3 B). Relative PtdIns*P* levels were five times higher in the hippocampus than in tsA201 cells (P value is 0.03, n = 5 samples for each cell type), while percentages of PtdIns and PtdIns(4,5)P_2 were not significantly different between cell types (P value for PtdIns is 0.1; P value for PtdIns(4,5)P_2 is 0.9). Statistical analyses used a one-way ANOVA with multiple comparisons for each phosphoinositide species between tsA201 cells and hippocampus extracts.

There are important considerations regarding this experiment. The proportion of phosphoinositides in the hippocampus is a combination of the lipids in neurons and other cell types, including astrocytes. Furthermore, these results were compared to those obtained using live-cell imaging of neurons in culture for 15 d. Hence, we have implicitly assumed that relative phosphoinositide abundance in hippocampal neurons at P1 is not significantly different from DIV15. Moreover, mass spectrometry does not distinguish the positions of phosphorylation on the inositol ring. Therefore, we were not able to distinguish regioisomers (i.e., PtdIns(4)*P* versus PtdIns(3)*P* or PtdIns(5)*P*). However, among the monophosphorylated regioisomers, PtdIns(4)*P* is the most abundant, being present in the PM, Golgi, and endosomes. Similarly, PtdIns(4,5)P_2 is the most abundant bisphosphorylated regioisomer (Wenk et al., 2003). Finally, significant PtdIns(4)*P* in our lipid extracts may be located in subcellular membranes.

From this result, we hypothesized that hippocampal neurons have a larger pool of PtdIns(4)*P*. To test this hypothesis, we quantified PtdIns(4)*P* in the PM and Golgi using P4M and FAPP1 probes, respectively. tsA201 cells showed a dim labeling of P4M intensity in the PM while the intensity of P4M in the PM of hippocampal neurons was significantly stronger (Fig. 3 C). The ratio (PM/cytosol) was 1.1 ± 0.7 for tsA201 cells and 1.6 ± 0.1 for hippocampal neurons (Fig. 3 D, n = 6, P = 0.0003). FAPP1, a sensor of PtdIns(4)*P* in Golgi, showed differential distribution in both cell types. While FAPP1 fluorescence was concentrated in a focal region in tsA201 cells, FAPP1 fluorescence was distributed in many intracellular bodies in hippocampal neurons (Fig. 3 E). Although the integrated fluorescence of FAPP1 was significantly lower in hippocampal neurons than for tsA201 cells (Fig. 3 F), the number of FAPP1 particles is significantly greater in hippocampal neurons (Fig. 3 G). We suggest that the difference in the distribution of the FAPP1 sensor between cell types limits our ability to discern whether the abundance of the PtdIns(4)*P* pool in Golgi is different. Together, the data suggest that hippocampal neurons have a larger pool of PtdIns(4)*P*, presumably at the level of the PM, leading to a faster resynthesis of PtdIns(4,5)P_2.

Stimulation of GqPCRs to activate PLC hydrolyzes both PtdIns(4,5)P_2 and PtdIns(4)*P*. PtdIns(4)*P* decreases by direct hydrolysis by PLC and by its use to replenish PtdIns(4,5)P_2 (Myeong et al., 2020; Traynor-Kaplan et al., 2017). We predicted that a larger pool of PtdIns(4)*P* in the PM may reduce or even prevent a significant depletion of PtdIns(4)*P* during glutamatergic or muscarinic stimulation. We tested this hypothesis by measuring the time course of P4M fluorescence intensity in the cytosol during the activation of receptors. Oxo-M induced a marked translocation of the P4M probe into the cytosol in tsA201 kidney cells (Fig. 3, H and I, n = 6), while L-Glu did not induce translocation of P4M in any of the hippocampal neurons tested (Fig. 3, J and K, n = 5). This result is in agreement with a large pool of PtdIns(4)*P* in the hippocampal neurons.

It has been proposed that PtdIns, the precursor of PtdIns(4)*P*, is poorly localized in the PM in mammalian cell lines (Pemberton et al., 2020; Zewe et al., 2020); however, its localization in neurons is unknown. Could hippocampal neurons have a large PtdIns pool in the PM that contributes to maintaining a large PtdIns(4)*P* pool? We explored and compared the localization of PtdIns pools in hippocampal neurons and tsA201 cells using the BcPI-PLC(ANH) probe. We did not observe measurable labeling of the BcPI-PLC(ANH) probe in the PM of either tsA201 cells or hippocampal neurons (Fig. 3 L). The localization of the BcPI-PLC(ANH) probe was observed in intracellular membranes, and the ratio of the signal relative to the cytosol (background signal) showed no difference between cell types (Fig. 3 M, n = 14, P = 0.16), ruling out the possibility of a bigger PtdIns pool in hippocampal neurons.

Large PtdIns(4)*P* pool supports fast resynthesis of PtdIns(4,5)P_2 in the presence of a PI4KIIIα inhibitor and in cells overexpressing M_1R

We tested the hypothesis of a large pool of PtdIns(4)*P* in hippocampal neurons by blocking PtdIns(4)*P* synthesis and studying PtdIns(4,5)P_2 resynthesis after oxo-M stimulation. Is PtdIns(4,5)P_2 resynthesized in hippocampal neurons without de

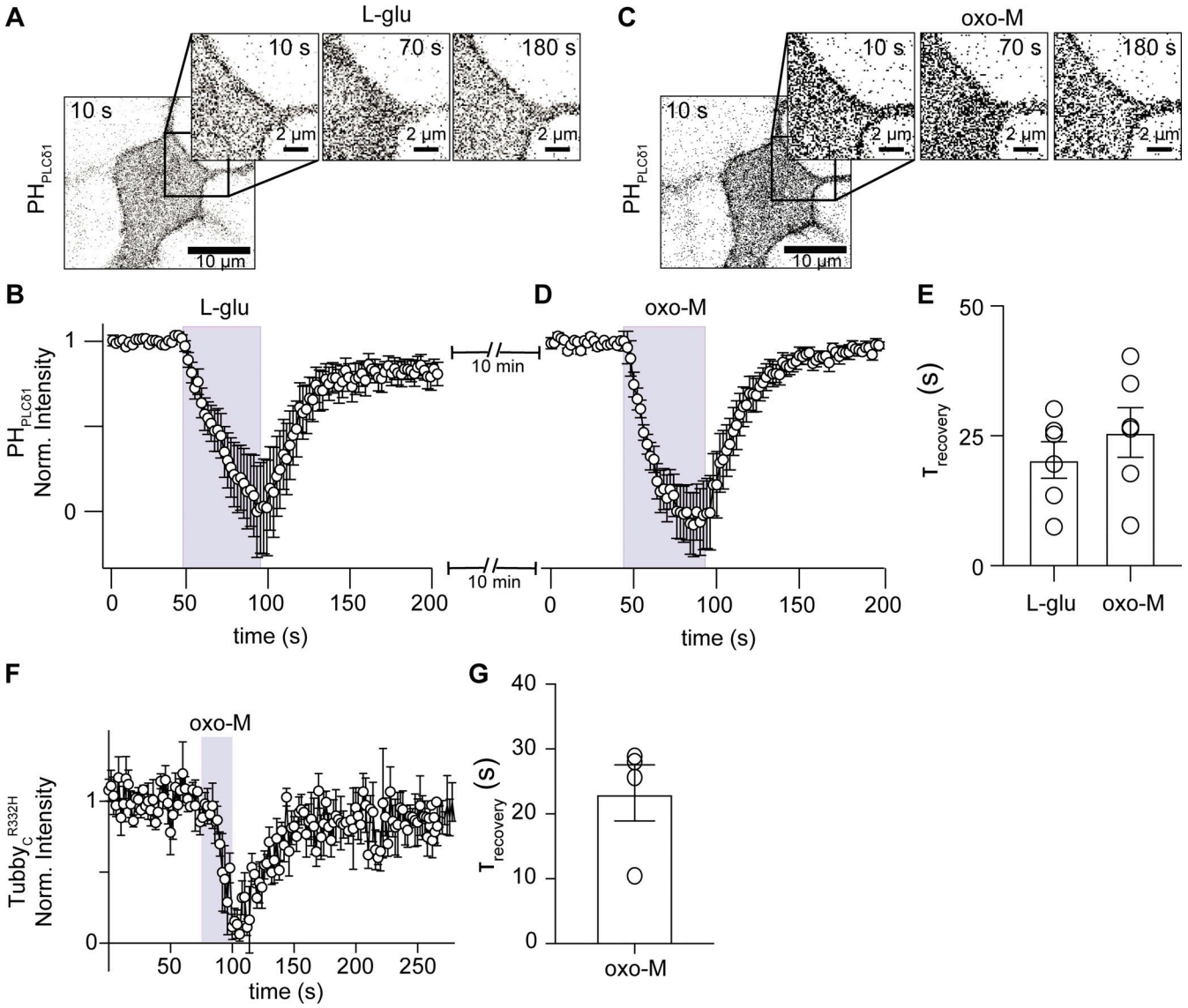

Figure 2. **Resynthesis of PtdIns(4,5)P_2 shows the same recovery kinetic after glutamatergic or muscarinic stimulation in hippocampal neurons.** This figure compares glutamate with muscarinic stimulation in the same cells; glutamate and muscarinic receptors are endogenously expressed. **(A and C)** Representative confocal images of $PH_{PLC\delta1}$ fluorescence (inverted contrast) from an isolated hippocampal neuron stimulated with 1 mM L-Glu (A) and then with 10 µM oxo-M (C). Muscarinic stimulation was carried out 10 min after the glutamatergic stimulation. **(B and D)** Average time courses of inverted normalized cytosolic intensity of $PH_{PLC\delta1}$ from isolated hippocampal neurons stimulated with L-Glu (B) or oxo (D). **(E)** Comparison of the exponential time constant of recovery as a proxy for PtdIns(4,5)P_2 resynthesis following glutamate or muscarinic stimulation in the same hippocampal neurons (n = 6). **(F)** Average time courses of inverted normalized cytosolic intensity of $Tubby_C^{R332H}$ from isolated hippocampal neurons stimulated with oxo-M. **(G)** Time constant of recovery following 10 µM oxo-M using $Tubby_C^{R332H}$ as PtdIns(4,5)P_2 sensor (n = 5).

novo PtdIns(4)P synthesis at the PM? As PI4KIIIα has been shown to be the enzyme responsible for PtdIns(4,5)P_2 synthesis in yeast and mammalian cells (Baird et al., 2008; Balla et al., 2008; Nakatsu et al., 2012; Stefan et al., 2011) and it has also been shown to be important for PtdIns(4)P synthesis at the PM in Schwann cells (Alvarez-Prats et al., 2018) and photoreceptors (Balakrishnan et al., 2018; Liu et al., 2018), it is likely that this enzyme is also responsible for PtdIns(4)P synthesis, and PtdIns(4,5)P_2 replenishment, in neurons.

To block PI4KIIIα, we treated the cells with GSK-A1 (Bojjireddy et al., 2014). We first measured changes in P4M fluorescence upon application of GSK-A1 and found that by 10 min, the signal ratio between the PM and the cytosol had decreased to about 0.25 (Fig. 4, A and B, n = 5). Next, we measured the time course of $PH_{PLC\delta1}$ translocation before and after bathing the cells in GSK-A1 for 10 min. In tsA201 cells, the recovery of PtdIns(4,5)P_2 after oxo-M was blocked after GSK-A1 treatment (Fig. 4, C and D). In the case of hippocampal neurons, the recovery of PtdIns(4,5)P_2 was unaffected by GSK-A1 (Fig. 4, E and F). The lack of the GSK-A1 effect opened an alternative hypothesis suggesting that PtdIns(4,5)P_2 replenishment in hippocampal neurons depends on a GSK-A1–insensitive isoform of PI4K. To verify whether GSK-A1 does influence PtdIns(4,5)P_2 resynthesis, we tested the effect of 50-min incubation in 100 nM

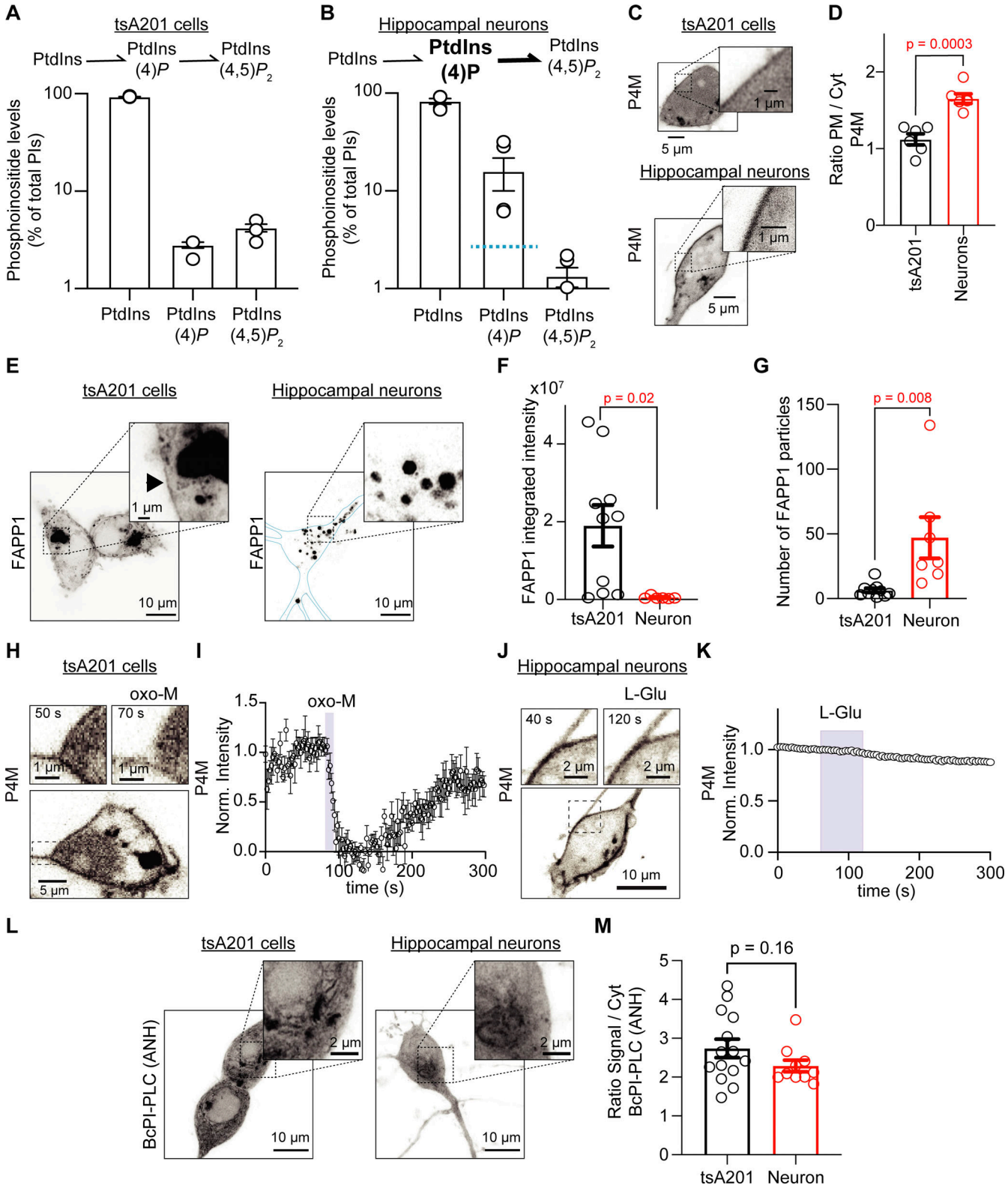

Figure 3. **PtdIns(4)*P* is relatively more abundant in hippocampal neurons than tsA201 cells and it is resistant to depletion. (A and B)** Histograms show the relative amounts of total PtdIns, PtdIns*P*, and PtdInsP_2 pools as percentages of total phosphoinositides for tsA201 cells (n = 3 dishes; A) and hippocampal neurons (n = 5 animals; B) determined by mass spectrometry. Blue line in B marks the percentage of PtdIns*P* in tsA201 cells for comparison. Note the logarithmic scale of phosphoinositide levels. **(C)** Representative confocal images of P4M fluorescence (inverted contrast) from a tsA201 cell and an isolated hippocampal neuron. **(D)** Ratio of mean fluorescence (PM/cytosol) of P4M in tsA201 cells and hippocampal neurons (n = 6 in each group). **(E)** Representative confocal images of FAPP1 fluorescence (inverted contrast) from a tsA201 cell and an isolated hippocampal neuron. Images show z-projections. Blue line delineates the PM. **(F)** Comparison of the integrated density of FAPP1-positive particles in tsA201 cells (n = 10) and hippocampal neurons (n = 7).

(G) Comparison of the number of FAPP1-positive particles in both cell types. **(H)** Representative images of P4M fluorescence (inverted contrast) from a tsA201 cell overexpressing M_1R stimulated with 10 µM oxo-M. **(I)** Average time course of inverted normalized cytosolic intensity of P4M from tsA201 cells as in H (n = 6). **(J)** Representative confocal images of P4M fluorescence (inverted contrast) from a hippocampal neuron stimulated with 1 mM L-Glu. **(K)** Average time course of inverted normalized cytosolic intensity of P4M from hippocampal neurons as in J (n = 5). Error bars are smaller than the data symbols. **(L)** Representative confocal images of BcPI-PLC(ANH) fluorescence (inverted contrast) from a tsA201 cell and an isolated hippocampal neuron. **(M)** Ratio of mean fluorescence (signal/cytosol) of BcPI-PLC(ANH) in tsA201 cells (n = 14) and hippocampal neurons (n = 10).

GSK-A1 on the rate of PtdIns(4,5)P_2 recovery and observed that this long treatment slowed down the recovery by 1.5-fold, from 17 ± 2 s to 25 ± 3 s (Fig. 4 G), suggesting that this enzyme does participate in the synthesis of PtdIns(4)P and PtdIns(4,5)P_2 in neurons. These results support the idea of a preexisting large pool of PtdIns(4)P capable of sustaining the fast PtdIns(4,5)P_2 resynthesis after receptor stimulation.

So far, we only considered as a primary explanation for the faster recovery of PtdIns(4,5)P_2, a large pool of PtdIns(4)P and have not tested alternative hypotheses. It has been shown that stimulating endogenous receptors activates PLC slightly enough to produce robust calcium signals without noticeable PtdIns(4,5)P_2 hydrolysis. On the other hand, overexpression increases the abundance of the same receptor 100-fold and completely depletes PtdIns(4,5)P_2 (Dickson et al., 2013). However, it has not been tested how the activation of a lower receptor density can influence the speed of PtdIns(4,5)P_2 resynthesis. Hence, we overexpressed M_1R in hippocampal neurons and measured the time course of PtdIns(4,5)P_2 during receptor stimulation. Overexpression of M_1R induced a robust decrease in PtdIns(4,5)P_2 levels as detected by the translocation of $PH_{PLC\delta1}$ (Fig. 4 H). Despite robust PtdIns(4,5)P_2 depletion, neurons overexpressing M_1R exhibited the same fast kinetics of recovery (27 ± 7 s, n = 5, Fig. 4 H), arguing against the idea that the fast PtdIns(4,5)P_2 recovery in hippocampal neurons is due to a lower PLC activation.

Since our working hypothesis was that there was a large PtdIns(4)P pool at the PM sustaining a fast PtdIns(4,5)P_2 resynthesis, we reasoned that depleting this pool by a stronger activation of PLC could unmask a different resynthesis kinetics. The overexpression of M_1R served this purpose. A second stimulation of overexpressed M_1R 5 min later depleted PtdIns(4,5)P_2 and led to a threefold slower recovery (150 ± 30 s, n = 5, Fig. 4 H), suggesting that, in hippocampal neurons, having a large PtdIns(4)P pool buffers the effect of PLC activation and allows faster PtdIns(4,5)P_2 recovery. This buffer is removed by a subsequent strong stimulation.

Computational model suggests altered enzymatic activity in hippocampal neurons to sustain a large PtdIns(4)P pool

For over a decade, the Hille lab has been developing a computational model to describe steady-state phosphoinositide metabolism, transient hydrolysis, and resynthesis of PtdIns(4)P and PtdIns(4,5)P_2. This model describes the signaling kinetics of phosphoinositide metabolism assuming that all reactions take place in the PM and follow nonsaturating linear kinetics. The activity of lipid kinases and phosphatases is assigned as a bulk activity rather than a molecular-specific activity, as we do not know the number or density of molecules. The model also reports the translocation of a PtdIns(4,5)P_2 sensor (e.g., $PH_{PLC\delta1}$) using a dissociation constant (Hirose et al., 1999; Lemmon et al., 1995; Winks et al., 2005; Xu et al., 2003). PtdIns(4,5)P_2 hydrolysis was modeled as described by Falkenburger et al. (2010) to reproduce an oxo-M concentration-response curve and time course (Jensen et al., 2009). The parameters of this model have been measured for both sympathetic neurons and tsA201 cells. We turned to this model to ask which parameters had to be modified to reproduce the percentages of phosphoinositides measured by mass spectrometry and the fast time constant of PtdIns(4,5)P_2 resynthesis measured with live imaging of the PtdIns(4,5)P_2 biosensor in hippocampal neurons. The model has multiple parameters that can be modified. Based on the experimental evidence presented in this work, we decided to first fit the parameters of pool size of each component, leaving intact the rate constants for PI4-K and PI4P-5K and the density of the receptors, PLC, and biosensors.

Our first modifications adjusted the densities of PtdIns, PtdIns(4)P, and PtdIns(4,5)P_2 to reproduce the percentages obtained by mass spectrometry. In the previous model, the PtdIns(4)P density was 4,000 molecules/µm^2, and the densities of PtdIns and PtdIns(4,5)P_2 were 140,000 and 5,000 molecules/µm^2, respectively (Falkenburger et al., 2010; Horowitz et al., 2005; Suh et al., 2004; Winks et al., 2005). Based on our measurements, we increased the density of PtdIns(4)P to 26,000 molecules/µm^2 and reduced the density of free PtdIns(4,5)P_2 to 2,400 molecules/µm^2 while keeping PtdIns constant, resulting in the following percentages for PtdIns, PtdIns(4)P, and PtdIns(4,5)P_2: 83.1%, 15.5%, and 1.4%, respectively (Fig. 5 A). In the model, these new phosphoinositide densities were unstable, with the PtdIns(4)P density decreasing and PtdIns(4,5)P_2 density increasing (Fig. 5, B and C). We achieved a stable steady state (Fig. 5, D and E) by increasing the rate of PtdIns(4)P synthesis while reducing the rate of its conversion to PtdIns(4,5)P_2. The equilibrium constant for the reaction to synthesize PtdIns(4)P increased by 44%, while the equilibrium constant for the reaction to synthesize PtdIns(4,5)P_2 decreased by 93%. Details of the parameters for every reaction can be found in Table S1.

Computational model recapitulates calcium dependence, degree of PLC activation, inability to deplete PtdIns(4)P, and effect of GSK-A1 in hippocampal neurons

Before assessing whether the changes in the proportions of lipids were enough to reproduce the observed faster kinetics, we modified the model further to include a reported calcium dependence of PLC. In tsA201 cells, PtdIns(4,5)P_2 is hydrolyzed even in the absence of external calcium (de la Cruz et al., 2020; Horowitz et al., 2005), although it is clear that calcium release from the stores and calcium entry through store-operated

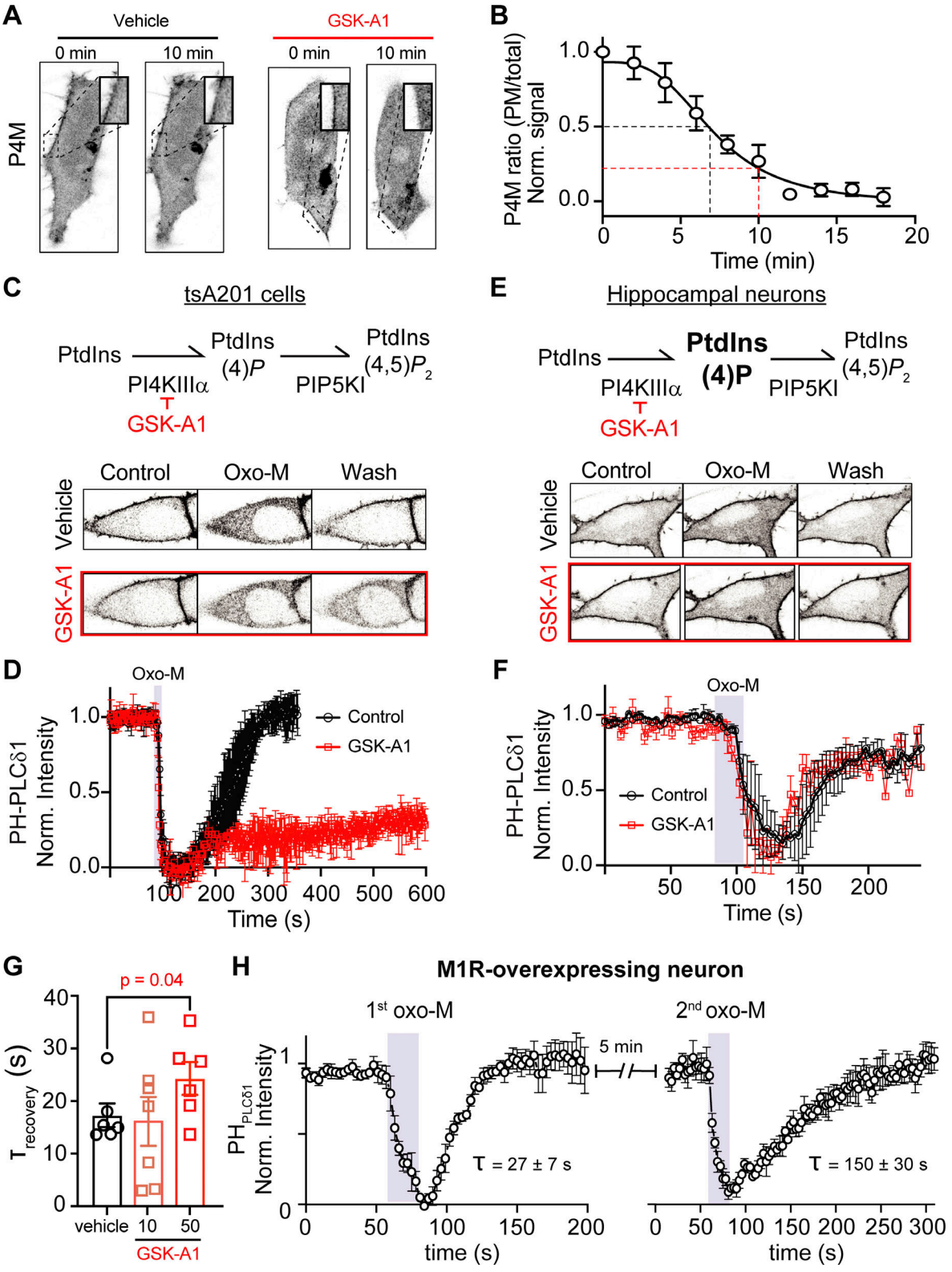

Figure 4. **Large PtdIns(4)*P* pool supports fast resynthesis of PtdIns(4,5)P_2 in the presence of a PI4KIIIα inhibitor and in cells overexpressing M_1R.** **(A)** Representative images of P4M fluorescence (inverted contrast) from tsA201 cells 10 min apart in the absence or presence of 100 nM GSK-A1. **(B)** Average P4M PM to total fluorescence ratio during GSK-A1 treatment. The black dashed line shows time at 50% decrease while the red line shows the decrease after 10 min treatment. **(C and E)** Representative images of $PH_{PLC\delta1}$ fluorescence (inverted contrast) from a tsA201 cell overexpressing M_1R (C) or a hippocampal neuron (E) stimulated with 10 µM oxo-M before and after 100 nM of GSK-A1 treatment (10 min). **(D and F)** Average time course of inverted normalized cytosolic intensity of $PH_{PLC\delta1}$ from tsA201 cells (D) and hippocampal neurons (F) stimulated with oxo-M before and after GSK-A1 treatment. **(G)** Tau recovery after oxo-M stimulation in the absence of GSK-A1 or after 10 and 50 min GSK-A1 treatment. **(H)** Average time course of inverted normalized cytosolic intensity of $PH_{PLC\delta1}$ from hippocampal neurons overexpressing the M_1R receptor. Neurons were treated two independent times with 5 min between applications. The average tau recovery for each stimulus is below each time course.

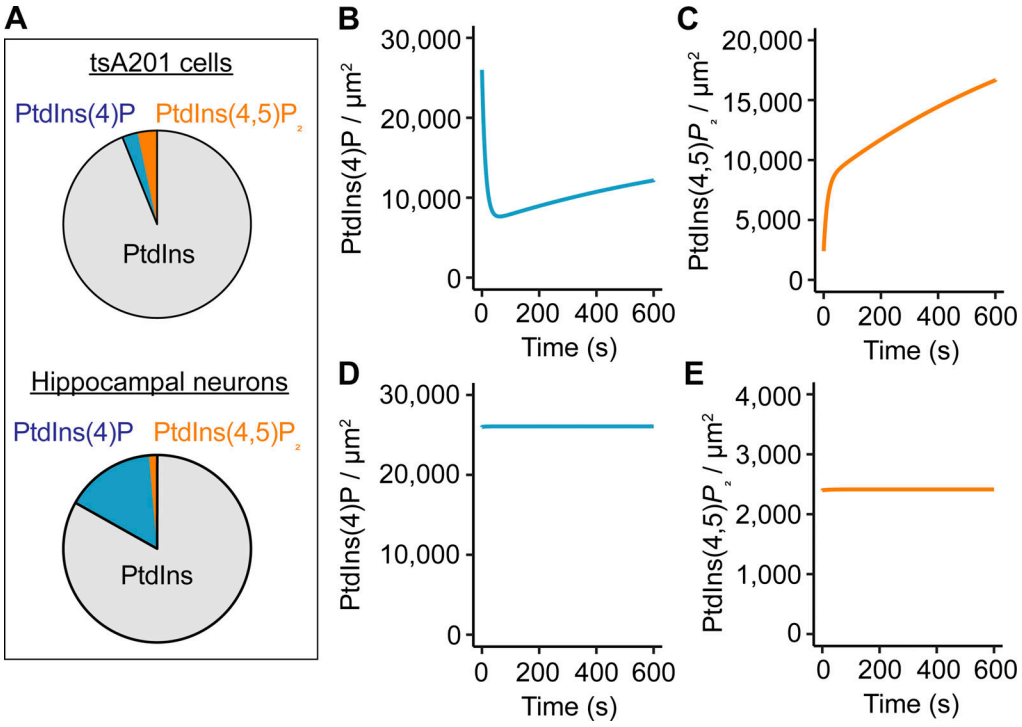

Figure 5. **Computational model suggests altered enzymatic activity in hippocampal neurons to sustain a large PtdIns(4)*P* pool. (A)** Comparison of in silico percentages of PtdIns, PtdIns(4)*P*, and PtdIns(4,5)P_2 in tsA201 cells and hippocampal neurons. **(B and C)** Simulated evolution of PtdIns(4)*P* (B) and PtdIns(4,5)P_2 (C) densities from starting conditions of 26,000 molecules/µm^2 (PtdIns(4)*P*) and 2,400 molecules/µm^2 (PtdIns(4,5)P_2) by using rate constants of the Falkenburger mathematical model of phosphosinositide metabolism in tsA201 cells. **(D and E)** Simulated evolution of PtdIns(4)*P* (D) and PtdIns(4,5)P_2 (E) densities in hippocampal neurons after adjustment of rate constants: increase of k_4K and decrease of k_5P (see details in Table S1).

calcium channels enhance PLC activity. In hippocampal neurons, the calcium dependence of PLC activity is more critical, as PtdIns(4,5)P_2 is not hydrolyzed in the absence of extracellular calcium (Kim et al., 2015; Kim et al., 1999). We experimentally confirmed that result by comparing glutamate-induced translocation of $PH_{PLC\delta1}$ in the presence or absence of calcium. We observed that repeating the stimulus 4 min later again elicited the translocation of $PH_{PLC\delta}$. Although the amount of translocation was reduced by 40%, it suggested that PLC was still activated. In contrast, the response was blunted when the second stimulus was applied in the absence of calcium (Fig. 6 A). In fact, every tested neuron showed a significant reduction of $PH_{PLC\delta1}$ translocation during the second application of glutamate in the absence of calcium (Fig. 6 B). Hence, calcium dependence was introduced in the model. The red line in Fig. 6 C shows the modeled time course of PtdIns(4,5)P_2 in the absence of extracellular calcium ions. Of consideration, we did not explore further whether PLC activation was due to calcium influx through ionotropic glutamate receptors or voltage-gated calcium channels nor did we perform a reversed experiment applying glutamate first in the absence of calcium and then in the presence of calcium.

We did not modify the model any further. We maintained the ability of PLC to hydrolyze PtdIns(4,5)P_2 and PtdIns(4)*P*, the density of PLC molecules as observed in sympathetic neurons, and the affinity constants of the sensors. Remarkably, the model reproduced a threefold faster resynthesis of PtdIns(4,5)P_2 in hippocampal neurons. The time constant of PtdIns(4,5)P_2 resynthesis obtained with the new model was 38.5 s (Fig. 6 D), in good agreement with the experimental value of 36.7 s (Fig. 1 D). Furthermore, the new model reproduced additional experimental observations without further modifications to the parameters. Our model reproduced the small change in $PH_{PLC\delta1}$ translocation, indicating that not all PtdIns(4,5)P_2 had been hydrolyzed (Fig. 6 C), and predicted that PLC depletes PtdIns(4,5)P_2 by only 10% upon receptor activation. The simulation of receptor activation also showed no significant translocation of the PtdIns(4)*P* reporter P4M from the PM (Fig. 6 E). However, magnification of the time of agonist application shows a small change in the reporter (Fig. 6 E, inset), suggesting that PLC is still capable of hydrolyzing PtdIns(4)*P* in the model for hippocampal neurons.

Following the experiment using GSK-A1, we modeled the inhibition of PI4KIIIα by GSK-A1 and assessed whether this inhibition would change the recovery kinetics in the model. First, we simulated different levels of PI4K inhibition in the tsA201 cell model and found that 90% of inhibition decreased the density of PtdIns(4)*P* at the PM to 20% (Fig. 6 F), similar to what was observed after 10 min of GSK-A1 application (Fig. 4 B). Surprisingly, the new model showed that this amount of PI4K inhibition did not change the kinetics of PtdIns(4,5)P_2 recovery in neurons (Fig. 6 G), similar to what was observed experimentally (Fig. 4 F). In summary, the mathematical model can explain the fast recovery of PtdIns(4,5)P_2 after receptor stimulation and

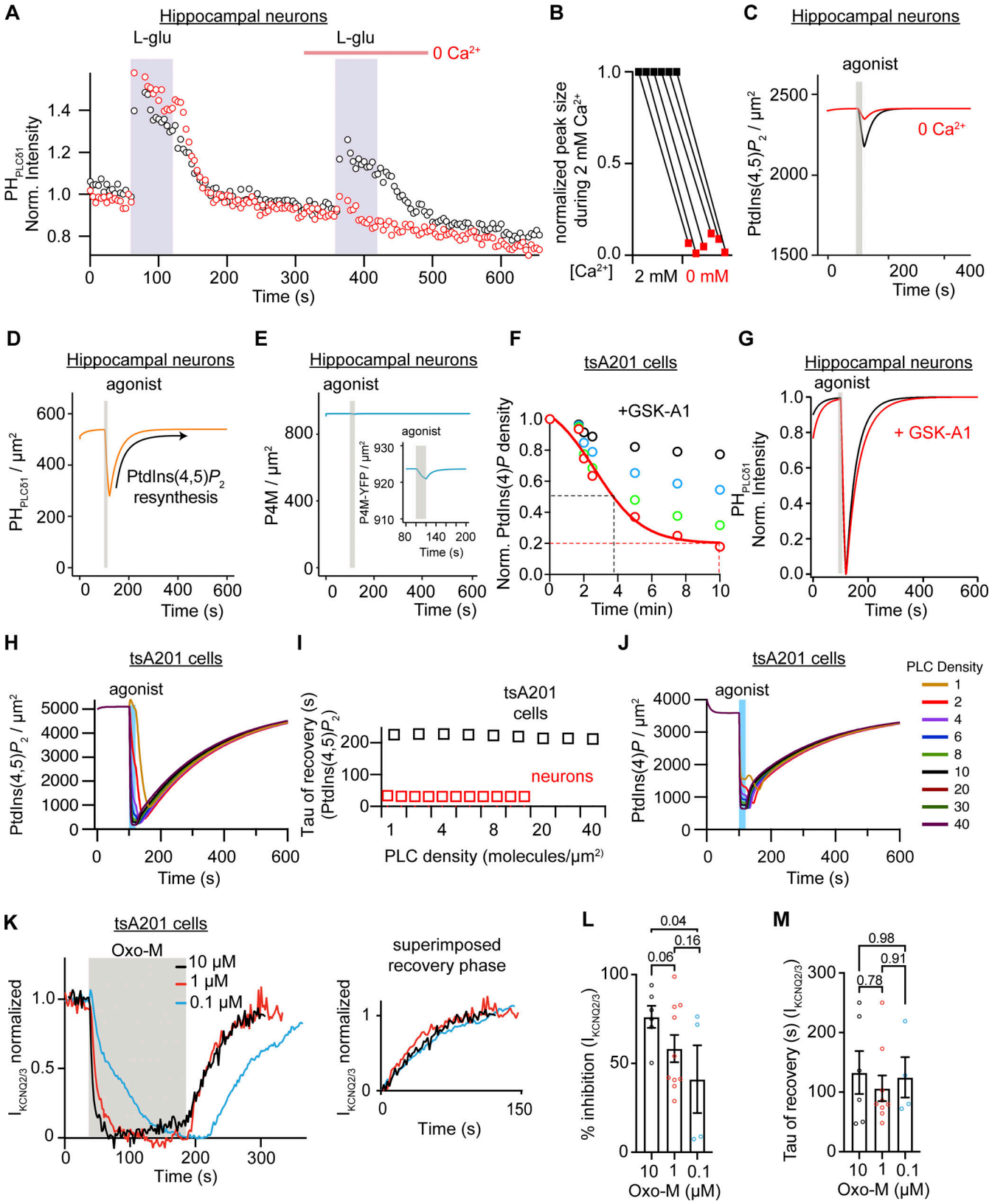

Figure 6. **Computational model recapitulates calcium dependence, degree of PLC activation, inability to deplete PtdIns(4)*P*, and effect of GSK-A1 in hippocampal neurons. (A)** Representative time courses of normalized cytosolic intensity of $PH_{PLC\delta1}$ in hippocampal neurons with two oxo-M stimulus in the presence (black) or absence (red) of extracellular calcium during the second oxo-M stimulation. **(B)** Comparison of the normalized peak of cytosolic $PH_{PLC\delta1}$ intensity by L-Glu before and after the removal of extracellular calcium (n = 6). **(C)** Simulated density of PtdIns(4,5)P_2 lipid at the PM in response to 1 mM L-Glu. The black line indicates simulation in the virtual presence of 2 mM extracellular calcium and the red line indicates simulation in the absence of extracellular

calcium. The gray bar indicates the time of simulated application of 1 mM L-Glu. **(D)** Simulated density of the $PH_{PLC\delta1}$ probe at the PM in response to 1 mM L-Glu. **(E)** Same simulation as described in D but showing density of the PtdIns(4)*P* sensor P4M at the PM. The inset shows an enlargement. **(F)** Simulated density of PtdIns(4)*P* in response to the inhibition of PI4KIIIα by GSK-A1 by 25% (black circles), 50% (blue circles), 75% (green circles), and 90% (red circles) over time. **(G)** Simulated normalized intensity of $PH_{PLC\delta1}$ at the PM of hippocampal neurons in response to PLC activation with (red trace) or without inhibition of PI4KIIIα by GSK-A1 (black trace). **(H)** Comparison of simulated density of PtdIns(4,5)P_2 in tsA201 cells with a varying density from 1 to 40 PLC molecules/μm^2. **(I)** Tau of simulated recovery of PtdIns(4,5)P_2 after PLC activation for different densities of PLC in hippocampal neurons (red squares) and tsA201 cells (black squares). **(J)** Same simulation as in H but showing density of PtdIns(4)*P*. **(K)** Average time course of KCNQ2/3 current upon application of 0.1, 1, and 10 μM of oxo-M. Inset compares the recovery phase. **(L)** Percentage of KCNQ2/3 current inhibition by 0.1, 1, and 10 μM of oxo-M. **(M)** Tau of recovery of KCNQ2/3 current from oxo-M inhibition.

recapitulates multiple additional experimental observations by only adjusting the levels of PtdIns(4)*P*.

Using the model, we again explored the alternative explanation that low PLC activation leads to fast PtdIns(4,5)P_2 synthesis, while strong PLC activation leads to slow PtdIns(4,5)P_2 recovery. We explored if the influence of varying PLC densities would impact the recovery kinetics of PtdIns(4)*P* and PtdIns(4,5)P_2 and evaluated if the activation of low PLC density makes a faster PtdIns(4,5)P_2 recovery in the tsA201 cell model. To test this possibility, we ran simulations with PLC densities ranging from 1 to 40 molecules/μm^2. A previous model used a value of 10 molecules/μm^2 when modelling the metabolism in tsA201 cells (Falkenburger et al., 2010) and we used 3 molecules/μm^2 in the SCG model (Kruse et al., 2016). We simulated a 20 s application of 10 μM oxo-M and did not change the receptor density, so the only variable was the PLC density. Fig. 6 H shows a family of time courses of PtdIns(4,5)P_2 at varying PLC densities. The amount of depletion decreased slightly and the time at which maximal depletion was reached was longer as PLC density decreased, but the recovery kinetics were similar (Fig. 6 I). We repeated this in silico experiment using the new model for hippocampal neurons. Varying the PLC density from 0.5 to 10 molecules/μm^2 did not alter the recovery kinetics either (Fig. 6 I). Interestingly, altering the levels of PLC from 40 to 1 molecules/μm^2 in the tsA201 model did not affect the amount of PtdIns(4)*P* reduction (Fig. 6 J), reinforcing the idea that a decrease in PLC density is not enough to explain the lack of PtdIns(4)*P* depletion observed in hippocampal neurons (Fig. 3 K). To further test the possibility that a small activation of PLC slows down the phase of PtdIns(4,5)P_2 recovery, we used lower concentrations of the agonist in tsA201 cells and measured KCNQ2/3 current as a proxy for PtdIns(4,5)P_2. Fig. 6 K shows time courses of KCNQ2/3 currents from cells treated with 10, 1, or 0.1 μM oxo-M. The agonist was applied for 120 s until the current reached a new steady state. Reducing the concentration of the agonist decreased the percentage of current inhibition (Fig. 6 L) but did not change the time constant of recovery (Fig. 6 M), suggesting that the magnitude of PLC activation does not affect the phase of PtdIns(4,5)P_2 resynthesis.

The resynthesis of PtdIns(4,5)P_2 is slower in astrocytes than hippocampal neurons

Astrocytes express muscarinic acetylcholine receptors coupled to $G_{\alpha q}$ (Araque et al., 2002; Shelton and McCarthy, 2000). We tested if the fast resynthesis of PtdIns(4,5)P_2 in hippocampal neurons was shared with astrocytes (Fig. 7 A). Application of oxo-M in astrocytes induced reversible translocation of the $PH_{PLC\delta1}$ sensor (Fig. 7 B). After washout of oxo-M, the sensor returned to the PM with a time constant of 71.0 ± 12.4 s (Fig. 7, C and D, n = 8). Astrocytes showed a delay before PtdIns(4,5)P_2 recovery and the mean of half-time recovery was 110 ± 20 s (Fig. 7 E, n = 8), suggesting an even longer time to resynthesize PtdIns(4,5)P_2 after agonist washout. PtdIns(4)*P* was observed in intracellular membranes without any labeling of the PM using FAPP1 and/or P4M sensors (Fig. 7, F and G). Thus, astrocytes seemingly resynthesize PtdIns(4,5)P_2 slower than hippocampal neurons. These results suggest that phosphoinositide metabolism may differ between cell types in the nervous system.

Discussion

At the beginning of this work, we were interested in testing the hypothesis that PtdIns(4,5)P_2 metabolism is cell-type specific and faster in neurons than in other cells. This required a parallel comparison between cell types using the same experimental strategy and setup. We have now compared the resynthesis of PtdIns(4,5)P_2 of hippocampal neurons to astrocytes and tsA201 cells. We found that hippocampal neurons can resynthesize PtdIns(4,5)P_2 quickly, two to three times faster than in astrocytes and tsA201 cells. These findings support our hypothesis.

What could be the physiological benefits of a fast PtdIns(4,5)P_2 synthesis for hippocampal neurons? We make a functional speculation. Both hippocampal neurons and astrocytes express metabotropic cholinergic receptors such as M_1R. Activation of cholinergic fibers innervating the hippocampus will activate neuronal and astrocytic M_1R, leading to PtdIns(4,5)P_2 depletion in all cells participating in synaptic communication (Fig. 7 A). We first describe the known functional effects of PtdIns(4,5)P_2 for each cell.

In neurons, PtdIns(4,5)P_2 regulates action potential firing patterns through controlling the activity of PtdIns(4,5)P_2-dependent ion channels, in particular KNCQ2/3 channels (Suh and Hille, 2002; Zhang et al., 2003). In hippocampal neurons, KCNQ2/3 channels control the threshold of action potential firing, oppose after depolarization, and consequently decrease endogenous burst firing and prevent repetitive firing (Brown and Passmore, 2009; Hu et al., 2007; Rasmussen et al., 2007; Shah et al., 2008). Net depletion of PtdIns(4,5)P_2 would therefore lead to hyperexcitability, increased action potential firing, and neurotransmitter release.

In addition, neurotransmitter release from presynaptic terminals is sustained by PtdIns(4,5)P_2 (Wenk et al., 2001), which is highly concentrated in microclusters (van den Bogaart et al., 2011). This dependence on PtdIns(4,5)P_2 is twofold. On the one

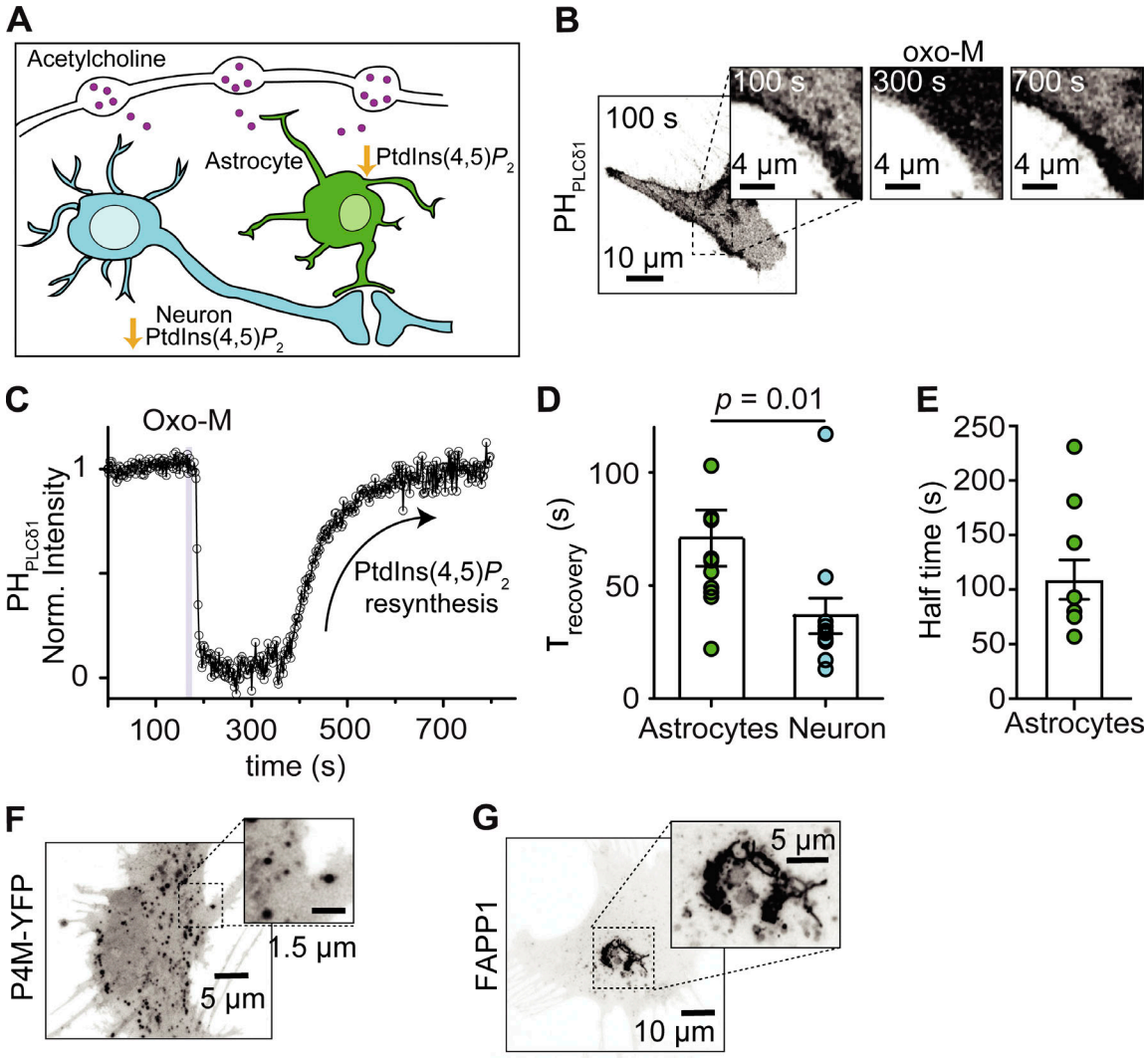

Figure 7. **The resynthesis of PtdIns(4,5)P_2 is slower in astrocytes than hippocampal neurons. (A)** Schematic showing that cholinergic stimulation is expected to promote PtdIns(4,5)P_2 depletion in both astrocytes and neurons. **(B)** Representative confocal images of $PH_{PLC\delta1}$ fluorescence (inverted contrast) from astrocytes stimulated with 10 µM oxo-M. **(C)** Representative time course of inverted normalized cytosolic intensity of $PH_{PLC\delta1}$ from the astrocyte shown in B. **(D)** Comparison of the exponential time constant of recovery as a proxy for PtdIns(4,5)P_2 resynthesis in astrocytes (n = 12) and hippocampal neurons (n = 12, data from Fig. 1 E). **(E)** Halftime recovery of $PH_{PLC\delta1}$ in astrocytes. **(F)** Representative confocal images of P4M fluorescence (inverted contrast) in an astrocyte. **(G)** Representative confocal images of FAPP1 fluorescence (inverted contrast) in an astrocyte.

hand, several synaptic proteins depend on PtdIns(4,5)P_2 to target the release site (Martin, 2012). For example, synaptotagmin-1 helps target neurotransmitter-containing vesicles to the release site through the interaction of the C2 domain with PtdIns(4,5)P_2. PtdIns(4,5)P_2 also interacts with the adaptor protein 2 (AP2), regulating the process of endocytosis (Antonescu et al., 2011). Hence, PtdIns(4,5)P_2 couples exocytosis and endocytosis (Koch and Holt, 2012). This role of PtdIns(4,5)P_2 in both exocytosis and endocytosis justifies why PtdIns(4,5)P_2 seems to control the releasable vesicle pool size (Milosevic et al., 2005). On the other hand, presynaptic calcium channels require PtdIns(4,5)P_2 to open (Suh et al., 2010). Action potentials arriving at axon terminals lead to calcium channel opening, calcium influx, and Ca^{2+}-triggered exocytosis. Therefore, G_qPCR-dependent PtdIns(4,5)P_2 hydrolysis in axon terminals is predicted to abolish neurotransmitter release.

In postsynaptic neurons, a few reports suggest that PtdIns(4,5)P_2 have an important role supporting synaptic plasticity. PLC activation and PtdIns(4,5)P_2 depletion is required for dendritic spine plasticity, long-term depression (Horne and Dell'Acqua, 2007), and long-term potentiation (Trovo et al., 2013).

Several types of synapses are covered by astrocytic membranes. Astrocytes participate in the synapse by regulating synaptic transmission and plasticity through the release of molecules such as ATP (Lalo et al., 2014; Pascual et al., 2005), D-serine (Papouin et al., 2017), and glutamate. Release of these molecules depends on the activation of the GPCR coupled to $G_{\alpha q}$, leading to calcium release from intracellular stores. Astrocytes express some PtdIns(4,5)P_2-dependent ion channels including TRPV channels and ionotropic purinergic P2X channels (Ase et al., 2010; Bernier et al., 2008; Verkhratsky and Nedergaard,

2018). Interestingly, the activation of P2X channels mediates the release of glial neurotransmitters (Duan and Neary, 2006; Suadicani et al., 2006). Therefore, M_1R-dependent PtdIns(4,5)P_2 hydrolysis is expected to first induce astrocyte glutamate release and then suppress astrocyte function by deactivating TRPV and P2X channels.

In short, cholinergic stimulation would result in PtdIns(4,5)P_2 depletion, which increases excitability of presynaptic neurons, controls exocytosis, promotes synaptic plasticity, and induces gliotransmitter release followed by suppression of astrocyte function. When the cholinergic stimulation ends, PtdIns(4,5)P_2 levels in neurons will recover quickly, returning circuit activity to its basal level. In contrast, PtdIns(4,5)P_2 levels in astrocytes require more time to return to their initial value. During this time, the participation of astrocytes in synaptic function might be reduced or absent. Therefore, the difference in kinetics of PtdIns(4,5)P_2 resynthesis may create a time window in which the synapse will not be influenced by astrocytes. As with cholinergic stimulation, agonists that activate other GPCRs coupled to $G_{\alpha q}$ in neurons or astrocytes are expected to lead to the same regulation. These agonists may include ATP, norepinephrine, and bradykinin. This scenario in the brain can be extended to other synapses where different cell types are involved, such as synapses between sympathetic neurons and their target organs.

We now turn to the mechanisms that account for the increased speed of PtdIns(4,5)P_2 synthesis observed in neurons compared to other cell types. The two types of neurons we have studied use different mechanisms to accelerate the synthesis of PtdIns(4,5)P_2. In the case of sympathetic neurons, the percentage of PtdIns(4)P is similar to that in previously studied cells, including tsA201 cells (Kruse et al., 2016). Percentages of 94% PtdIns, 3% PtdIns(4)P, and 3% PtdIns(4,5)P_2 have been reported in N1E-115 and SH-SY5Y cells (Balakrishnan et al., 2018; Lemmon, 2008; Willars et al., 1998; Xu et al., 2003). Therefore, we proposed that in sympathetic neurons, fast synthesis of PtdIns(4,5)P_2 is due to an increased lipid kinase activity upon activation of the receptor. Unlike sympathetic neurons, hippocampal neurons have an increased reserve of PtdIns(4)P relative to PtdIns(4,5)P_2 under resting conditions, and hence, PtdIns(4,5)P_2 metabolism is different even between neurons. Interestingly, it has been reported that neurons from the dentate gyrus have such a rapid resynthesis of PtdIns(4,5)P_2 that cholinergic stimulation leads to an increase rather than a depletion of PtdIns(4,5)P_2 (Carver and Shapiro, 2019).

Interestingly, in both sympathetic and hippocampal neurons, the mechanism underlying more rapid PtdIns(4,5)P_2 synthesis compared to tsA201 cells involves acceleration of PtdIns(4)P synthesis from PtdIns by PI4K, rather than an increase in the activity of PIP5K. Using the mathematical model adjusted for the kinetics of PtdIns(4,5)P_2 synthesis in sympathetic neurons, we had predicted a threefold acceleration of PI4K synthesis compared to tsA201 cells. The model for hippocampal neurons predicts a ninefold acceleration of PtdIns(4)P synthesis compared to sympathetic neurons or 28-fold compared to tsA201 cells. This increase, in combination with the available PtdIns(4)P pool, is sufficient to synthesize PtdIns(4,5)P_2 quickly. Interestingly, PtdIns(4)P is depleted in sympathetic neurons when cholinergic receptors are stimulated, causing a delay in PtdIns(4,5)P_2 resynthesis (Kruse et al., 2016). In hippocampal neurons, PtdIns(4)P is not depleted significantly upon PLC activation. One might envision several explanations for this result. A reduction in the receptor or PLC density could lead to less PtdIns(4,5)P_2 depletion and an undetectable change in PtdIns(4)P. However, we did not need to change any of these parameters in the model to account for the observations. In fact, modeling an increase in the density of PLC was not enough to deplete PtdIns(4)P or change the time course of PtdIns(4,5)P_2 synthesis. Therefore, we concluded that the acceleration of the metabolic step representing the activation of PI4K allows for stable higher levels of PtdIns(4)P under resting conditions and suffices to reproduce the lack of PtdIns(4)P depletion without further assumptions.

What are the potential mechanisms to explain a higher PtdIns(4)P pool? In the model, the rate constant representing the synthesis of PtdIns(4)P lumps diverse cellular processes, including the abundance of PI4K and its enzymatic activity. In fact, the rate constant groups all PI4K types contributing to PtdIns(4)P synthesis. In multiple cells, the specific enzyme responsible for synthesizing PtdIns(4)P at the PM is PI4KIIIα (Alvarez-Prats et al., 2018; Baird et al., 2008; Balakrishnan et al., 2018; Balla et al., 2008; Liu et al., 2018; Nakatsu et al., 2012; Stefan et al., 2011). By inhibiting this enzyme with GSK-A1 (Bojjireddy et al., 2014), we showed that PtdIns(4,5)P_2 can still be replenished, in agreement with the idea of a larger pool of PtdIns(4)P at the PM. Interestingly, long GSK-A1 treatment (50 min) slows the PtdIns(4,5)P_2 recovery after muscarinic activation, suggesting that this enzyme does participate in the synthesis of PtdIns(4)P and PtdIns(4,5)P_2 in neurons. However, we cannot discard the possibility that, in addition to PI4KIIIα, other types of PI4K maintain the large pool of PtdIns(4)P at the PM. Our model does not discriminate against other PtdIns(4)P sources such as the vesicular transport of PtdIns(4)P from the Golgi to the PM or the activity of lipid transfer proteins acting at membrane contact sites between organelles. These lipid transfer proteins are, for example, supplying PtdIns to the PM. Two recent papers have shown that PtdIns is not abundant at the PM. Instead, it localized to internal membranes (Pemberton et al., 2020; Zewe et al., 2020). Hence, the supply of PtdIns to the PM to be used by PI4Ks essential for the rate of PtdIns(4,5)P_2 synthesis. This reaction is balanced by the dephosphorylation of PtdIns(4)P to synthesize PtdIns by PtdIns(4)P phosphatase, Sac1. Then, we expect that Sac1 activity in hippocampal neurons is relatively low. A future characterization of the contributions of these individual processes will provide further insight into the cellular mechanism governing a large PtdIns(4)P pool in hippocampal neurons.

Data availability

The code for the newly generated model is available on GitHub at the link https://github.com/Martin-Kruse/rat_hippocampus_PI_metabolism.

Acknowledgments

Joseph A. Mindell served as editor.

We thank Bertil Hille for his contribution to funding, editing, and writing of this project. We thank readers Andres Barria, Jill Jensen, Seung-Ryoung Jung, Duk-Su Koh, and Jongyun Myeong for feedback on the manuscript; Lea Miller for technical assistance; and Dale Whittington, Alexis Traynor-Kaplan, and other members of the University of Washington School of Pharmacy Mass Spectrometry Center for their contribution to lipid measurements.

This study was supported by the University of Washington Start-up Funds (to O. Vivas), the National Institutes of Health MIRA R35 GM142690 to O. Vivas, R37-NS08174 to Bertil Hille, the Wayne E. Crill Endowed Professorship (to Bertil Hille), and an Institutional Development Award (IDeA) from the National Institute of General Medical Sciences of the National Institutes of Health under grant number P20GM103423 (to M. Kruse). C. Kushmerick was supported by a Fellowship from CNPq (201815/2015-0) and grants from FAPEMIG (APQ-02013-15) and CNPq (301798/2019-2).

The authors declare no competing financial interests.

Author contributions: L. de la Cruz, formal analysis, investigation, and writing original draft. C. Kushmerick, formal analysis, investigation, methodology, and writing reviewing and editing. J.M. Sullivan, investigation, methodology, and writing reviewing and editing. M. Kruse, conceptualization, data curation, formal analysis, investigation, methodology, writing original draft, and reviewing and editing. O. Vivas, conceptualization, data curation, formal analysis, investigation, methodology, writing original draft, reviewing and editing, funding acquisition, and project administration.

Submitted: 20 July 2021
Revised: 1 January 2022
Accepted: 24 January 2022

References

Alvarez-Prats, A., I. Bjelobaba, Z. Aldworth, T. Baba, D. Abebe, Y.J. Kim, S.S. Stojilkovic, M. Stopfer, and T. Balla. 2018. Schwann-cell-specific deletion of phosphatidylinositol 4-kinase alpha causes aberrant myelination. *Cell Rep.* 23:2881–2890. https://doi.org/10.1016/j.celrep.2018.05.019.

Antonescu, C.N., F. Aguet, G. Danuser, and S.L. Schmid. 2011. Phosphatidylinositol-(4,5)-bisphosphate regulates clathrin-coated pit initiation, stabilization, and size. *Mol. Biol. Cell.* 22:2588–2600. https://doi.org/10.1091/mbc.e11-04-0362

Araque, A., E.D. Martin, G. Perea, J.I. Arellano, and W. Buno. 2002. Synaptically released acetylcholine evokes Ca2+ elevations in astrocytes in hippocampal slices. *J. Neurosci.* 22:2443–2450. https://doi.org/10.1523/JNEUROSCI.22-07-02443.2002.

Ase, A.R., L.P. Bernier, D. Blais, Y. Pankratov, and P. Seguela. 2010. Modulation of heteromeric P2X1/5 receptors by phosphoinositides in astrocytes depends on the P2X1 subunit. *J. Neurochem.* 113:1676–1684. https://doi.org/10.1111/j.1471-4159.2010.06734.x

Baird, D., C. Stefan, A. Audhya, S. Weys, and S.D. Emr. 2008. Assembly of the PtdIns 4-kinase Stt4 complex at the plasma membrane requires Ypp1 and Efr3. *J. Cell Biol.* 183:1061–1074. https://doi.org/10.1083/jcb.200804003

Balakrishnan, S.S., U. Basu, D. Shinde, R. Thakur, M. Jaiswal, and P. Raghu. 2018. Regulation of PI4P levels by PI4KIIIα during G-protein-coupled PLC signaling in Drosophila photoreceptors. *J. Cell Sci.*. 131:jcs217257. [Replaced doi from CrossRef] [CS: 100]. https://doi.org/10.1242/jcs.217257.

Balla, A., Y.J. Kim, P. Varnai, Z. Szentpetery, Z. Knight, K.M. Shokat, and T. Balla. 2008. Maintenance of hormone-sensitive phosphoinositide pools in the plasma membrane requires phosphatidylinositol 4-kinase IIIalpha. *Mol. Biol. Cell.* 19:711–721. https://doi.org/10.1091/mbc.e07-07-0713

Bernier, L.P., A.R. Ase, S. Chevallier, D. Blais, Q. Zhao, E. Boue-Grabot, D. Logothetis, and P. Seguela. 2008. Phosphoinositides regulate P2X4 ATP-gated channels through direct interactions. *J. Neurosci.* 28:12938–12945. https://doi.org/10.1523/jneurosci.3038-08.2008

Bojjireddy, N., J. Botyanszki, G. Hammond, D. Creech, R. Peterson, D.C. Kemp, M. Snead, R. Brown, A. Morrison, S. Wilson, et al. 2014. Pharmacological and genetic targeting of the PI4KA enzyme reveals its important role in maintaining plasma membrane phosphatidylinositol 4-phosphate and phosphatidylinositol 4,5-bisphosphate levels. *J. Biol. Chem.* 289:6120–6132. https://doi.org/10.1074/jbc.m113.531426

Brewer, G.J., J.R. Torricelli, E.K. Evege, and P.J. Price. 1993. Optimized survival of hippocampal neurons in B27-supplemented Neurobasal, a new serum-free medium combination. *J. Neurosci. Res.* 35:567–576. https://doi.org/10.1002/jnr.490350513

Brown, D.A., and G.M. Passmore. 2009. Neural KCNQ (Kv7) channels. *Br. J. Pharmacol.* 156:1185–1195. https://doi.org/10.1111/j.1476-5381.2009.00111.x

Carver, C.M., and M.S. Shapiro. 2019. Gq-coupled muscarinic receptor enhancement of KCNQ2/3 channels and activation of TRPC channels in multimodal control of excitability in dentate gyrus granule cells. *J. Neurosci.* 39:1566–1587. https://doi.org/10.1523/jneurosci.1781-18.2018

de la Cruz, L., A. Traynor-Kaplan, O. Vivas, B. Hille, and J.B. Jensen. 2020. Plasma membrane processes are differentially regulated by type I phosphatidylinositol phosphate 5-kinases and RASSF4. *J. Cell Sci.* 133:jcs233254. https://doi.org/10.1242/jcs.233254

Dickson, E.J., B.H. Falkenburger, and B. Hille. 2013. Quantitative properties and receptor reserve of the IP(3) and calcium branch of G(q)-coupled receptor signaling. *J. Gen. Physiol.* 141:521–535. https://doi.org/10.1085/jgp.201210886

Duan, S., and J.T. Neary. 2006. P2X(7) receptors: properties and relevance to CNS function. *Glia.* 54:738–746. https://doi.org/10.1002/glia.20397

Falkenburger, B.H., J.B. Jensen, and B. Hille. 2010. Kinetics of PIP2 metabolism and KCNQ2/3 channel regulation studied with a voltage-sensitive phosphatase in living cells. *J. Gen. Physiol.* 135:99–114. https://doi.org/10.1085/jgp.200910345

Gresset, A., J. Sondek, and T.K. Harden. 2012. The phospholipase C isozymes and their regulation. *Subcell Biochem.* 58:61–94. https://doi.org/10.1007/978-94-007-3012-0_3.

Hackelberg, S., and D. Oliver. 2018. Metabotropic acetylcholine and glutamate receptors mediate PI(4,5)P(2) depletion and oscillations in hippocampal CA1 pyramidal neurons in situ. *Sci. Rep.* 8:12987. https://doi.org/10.1038/s41598-018-31322-8

Hammond, G.R., M.P. Machner, and T. Balla. 2014. A novel probe for phosphatidylinositol 4-phosphate reveals multiple pools beyond the Golgi. *J. Cell Biol.* 205:113–126. https://doi.org/10.1083/jcb.201312072

Hille, B., E.J. Dickson, M. Kruse, O. Vivas, and B.C. Suh. 2015. Phosphoinositides regulate ion channels. *Biochim. Biophys. Acta.* 1851:844–856. https://doi.org/10.1016/j.bbalip.2014.09.010

Hirose, K., S. Kadowaki, M. Tanabe, H. Takeshima, and M. Iino. 1999. Spatiotemporal dynamics of inositol 1,4,5-trisphosphate that underlies complex Ca^{2+} mobilization patterns. *Science.* 284:1527–1530. https://doi.org/10.1126/science.284.5419.1527

Horne, E.A., and M.L. Dell'Acqua. 2007. Phospholipase C is required for changes in postsynaptic structure and function associated with NMDA receptor-dependent long-term depression. *J. Neurosci.* 27:3523–3534. https://doi.org/10.1523/jneurosci.4340-06.2007

Horowitz, L.F., W. Hirdes, B.C. Suh, D.W. Hilgemann, K. Mackie, and B. Hille. 2005. Phospholipase C in living cells: activation, inhibition, Ca2+ requirement, and regulation of M current. *J. Gen. Physiol.* 126:243–262. https://doi.org/10.1085/jgp.200509309

Hu, H., K. Vervaeke, and J.F. Storm. 2007. M-channels (Kv7/KCNQ channels) that regulate synaptic integration, excitability, and spike pattern of CA1 pyramidal cells are located in the perisomatic region. *J. Neurosci.* 27:1853–1867. https://doi.org/10.1523/jneurosci.4463-06.2007

Jensen, J.B., J.S. Lyssand, C. Hague, and B. Hille. 2009. Fluorescence changes reveal kinetic steps of muscarinic receptor-mediated modulation of phosphoinositides and Kv7.2/7.3 K+ channels. *J. Gen. Physiol.* 133:347–359. https://doi.org/10.1085/jgp.200810075

Kim, H.H., K.H. Lee, D. Lee, Y.E. Han, S.H. Lee, J.W. Sohn, and W.K. Ho. 2015. Costimulation of AMPA and metabotropic glutamate receptors underlies phospholipase C activation by glutamate in hippocampus. *J. Neurosci.* 35:6401–6412. https://doi.org/10.1523/jneurosci.4208-14.2015

Kim, Y.H., T.J. Park, Y.H. Lee, K.J. Baek, P.G. Suh, S.H. Ryu, and K.T. Kim. 1999. Phospholipase C-delta1 is activated by capacitative calcium entry

that follows phospholipase C-beta activation upon bradykinin stimulation. *J. Biol. Chem.* 274:26127–26134. https://doi.org/10.1074/jbc.274.37.26127

Koch, M., and M. Holt. 2012. Coupling exo- and endocytosis: an essential role for PIP_2 at the synapse. *Biochim. Biophys. Acta.* 1821:1114–1132. https://doi.org/10.1016/j.bbalip.2012.02.008

Kruse, A.C., B.K. Kobilka, D. Gautam, P.M. Sexton, A. Christopoulos, and J. Wess. 2014. Muscarinic acetylcholine receptors: novel opportunities for drug development. *Nat. Rev. Drug Discov.* 13:549–560. https://doi.org/10.1038/nrd4295

Kruse, M., O. Vivas, A. Traynor-Kaplan, and B. Hille. 2016. Dynamics of phosphoinositide-dependent signaling in sympathetic neurons. *J. Neurosci.* 36:1386–1400. https://doi.org/10.1523/jneurosci.3535-15.2016

Lalo, U., O. Palygin, S. Rasooli-Nejad, J. Andrew, P.G. Haydon, Y. Pankratov. 2014. Exocytosis of ATP from astrocytes modulates phasic and tonic inhibition in the neocortex. *PLoS Biol.* 12:e1001747. https://doi.org/10.1371/journal.pbio.1001747

Lemmon, M.A. 2008. Membrane recognition by phospholipid-binding domains. *Nat. Rev. Mol. Cell Biol.* 9:99–111. https://doi.org/10.1038/nrm2328

Lemmon, M.A., K.M. Ferguson, R. O'Brien, P.B. Sigler, and J. Schlessinger. 1995. Specific and high-affinity binding of inositol phosphates to an isolated pleckstrin homology domain. *Proc. Natl. Acad. Sci. USA.* 92:10472–10476. https://doi.org/10.1073/pnas.92.23.10472

Liu, C.H., M.K. Bollepalli, S.V. Long, S. Asteriti, J. Tan, J.A. Brill, and R.C. Hardie. 2018. Genetic dissection of the phosphoinositide cycle in Drosophila photoreceptors. *J. Cell Sci.* 131:jcs214478. https://doi.org/10.1242/jcs.214478

Martin, T.F. 2012. Role of PI(4,5)P(2) in vesicle exocytosis and membrane fusion. *Subcell. Biochem.* 59:111–130. https://doi.org/10.1007/978-94-007-3015-1

Milosevic, I., J.B. Sørensen, T. Lang, M. Krauss, G. Nagy, V. Haucke, R. Jahn, and E. Neher. 2005. Plasmalemmal phosphatidylinositol-4,5-bisphosphate level regulates the releasable vesicle pool size in chromaffin cells. *J. Neurosci.* 25:2557–2565. https://doi.org/10.1523/jneurosci.3761-04.2005

Myeong, J., L. de la Cruz, S.R. Jung, J.H. Yeon, B.C. Suh, D.S. Koh, B. Hille. 2020. Phosphatidylinositol 4,5-bisphosphate is regenerated by speeding of the PI 4-kinase pathway during long PLC activation. *J. Gen. Physiol.* 152:e202012627. https://doi.org/10.1085/jgp.202012627

Nakatsu, F., J.M. Baskin, J. Chung, L.B. Tanner, G. Shui, S.Y. Lee, M. Pirruccello, M. Hao, N.T. Ingolia, M.R. Wenk, and P. De Camilli. 2012. PtdIns4P synthesis by PI4KIIIα at the plasma membrane and its impact on plasma membrane identity. *J. Cell Biol.* 199:1003–1016. https://doi.org/10.1083/jcb.201206095

Olivença, D.V., I. Uliyakina, L.L. Fonseca, M.D. Amaral, E.O. Voit, and F.R. Pinto. 2018. A mathematical model of the phosphoinositide pathway. *Sci. Rep.* 8:3904. https://doi.org/10.1038/s41598-018-22226-8

Papouin, T., J.M. Dunphy, M. Tolman, K.T. Dineley, and P.G. Haydon. 2017. Septal cholinergic neuromodulation tunes the astrocyte-dependent gating of hippocampal NMDA receptors to wakefulness. *Neuron.* 94:840–854.e7. https://doi.org/10.1016/j.neuron.2017.04.021

Pascual, O., K.B. Casper, C. Kubera, J. Zhang, R. Revilla-Sanchez, J.Y. Sul, H. Takano, S.J. Moss, K. McCarthy, and P.G. Haydon. 2005. Astrocytic purinergic signaling coordinates synaptic networks. *Science.* 310:113–116. https://doi.org/10.1126/science.1116916

Pemberton, J.G., Y.J. Kim, J. Humpolickova, A. Eisenreichova, N. Sengupta, D.J. Toth, E. Boura, T. Balla. 2020. Defining the subcellular distribution and metabolic channeling of phosphatidylinositol. *J. Cell Biol.* 219:e201906130. https://doi.org/10.1083/jcb.201906130

Pratt, K.G., E.C. Zimmerman, D.G. Cook, and J.M. Sullivan. 2011. Presenilin 1 regulates homeostatic synaptic scaling through Akt signaling. *Nat. Neurosci.* 14:1112–1114. https://doi.org/10.1038/nn.2893

Quinn, K.V., P. Behe, and A. Tinker. 2008. Monitoring changes in membrane phosphatidylinositol 4,5-bisphosphate in living cells using a domain from the transcription factor tubby. *J. Physiol.* 586:2855–2871. https://doi.org/10.1113/jphysiol.2008.153791

Raghu, P., A. Joseph, H. Krishnan, P. Singh, and S. Saha. 2019. Phosphoinositides: regulators of nervous system function in health and disease. *Front. Mol. Neurosci.* 12:208. https://doi.org/10.3389/fnmol.2019.00208

Rasmussen, H.B., C. Frokjaer-Jensen, C.S. Jensen, H.S. Jensen, N.K. Jorgensen, H. Misonou, J.S. Trimmer, S.P. Olesen, and N. Schmitt. 2007. Requirement of subunit co-assembly and ankyrin-G for M-channel localization at the axon initial segment. *J. Cell Sci.* 120:953–963. https://doi.org/10.1242/jcs.03396

Rohács, T., C.M. Lopes, I. Michailidis, and D.E. Logothetis. 2005. PI(4,5)P2 regulates the activation and desensitization of TRPM8 channels through the TRP domain. *Nat. Neurosci.* 8:626–634. https://doi.org/10.1038/nn1451

Rosenbaum, D.M., S.G. Rasmussen, and B.K. Kobilka. 2009. The structure and function of G-protein-coupled receptors. *Nature.* 459:356–363. https://doi.org/10.1038/nature08144

Schindelin, J., I. Arganda-Carreras, E. Frise, V. Kaynig, M. Longair, T. Pietzsch, S. Preibisch, C. Rueden, S. Saalfeld, B. Schmid, et al. 2012. Fiji: an open-source platform for biological-image analysis. *Nat. Methods.* 9:676–682. https://doi.org/10.1038/nmeth.2019

Shah, M.M., M. Migliore, I. Valencia, E.C. Cooper, and D.A. Brown. 2008. Functional significance of axonal Kv7 channels in hippocampal pyramidal neurons. *Proc. Natl. Acad. Sci. USA.* 105:7869–7874. https://doi.org/10.1073/pnas.0802805105

Shelton, M.K., and K.D. McCarthy. 2000. Hippocampal astrocytes exhibit Ca2+-elevating muscarinic cholinergic and histaminergic receptors in situ. *J. Neurochem.* 74:555–563. https://doi.org/10.1046/j.1471-4159.2000.740555.x

Stauffer, T.P., S. Ahn, and T. Meyer. 1998. Receptor-induced transient reduction in plasma membrane PtdIns(4,5)P2 concentration monitored in living cells. *Curr. Biol.* 8:343–346. https://doi.org/10.1016/s0960-9822(98)70135-6

Stefan, C.J., A.G. Manford, D. Baird, J. Yamada-Hanff, Y. Mao, and S.D. Emr. 2011. Osh proteins regulate phosphoinositide metabolism at ER-plasma membrane contact sites. *Cell.* 144:389–401. https://doi.org/10.1016/j.cell.2010.12.034

Suadicani, S.O., C.F. Brosnan, and E. Scemes. 2006. P2X7 receptors mediate ATP release and amplification of astrocytic intercellular Ca2+ signaling. *J. Neurosci.* 26:1378–1385. https://doi.org/10.1523/jneurosci.3902-05.2006

Suh, B.C., and B. Hille. 2002. Recovery from muscarinic modulation of M current channels requires phosphatidylinositol 4,5-bisphosphate synthesis. *Neuron.* 35:507–520. https://doi.org/10.1016/s0896-6273(02)00790-0

Suh, B.C., L.F. Horowitz, W. Hirdes, K. Mackie, and B. Hille. 2004. Regulation of KCNQ2/KCNQ3 current by G protein cycling: the kinetics of receptor-mediated signaling by gq. *J. Gen. Physiol.* 123:663–683. https://doi.org/10.1085/jgp.200409029

Suh, B.C., K. Leal, and B. Hille. 2010. Modulation of high-voltage activated Ca(2+) channels by membrane phosphatidylinositol 4,5-bisphosphate. *Neuron.* 67:224–238. https://doi.org/10.1016/j.neuron.2010.07.001

Szentpetery, Z., A. Balla, Y.J. Kim, M.A. Lemmon, and T. Balla. 2009. Live cell imaging with protein domains capable of recognizing phosphatidylinositol 4,5-bisphosphate; a comparative study. *BMC Cell Biol.* 10:67. https://doi.org/10.1186/1471-2121-10-67

Traynor-Kaplan, A., M. Kruse, E.J. Dickson, G. Dai, O. Vivas, H. Yu, D. Whittington, and B. Hille. 2017. Fatty-acyl chain profiles of cellular phosphoinositides. *Biochim. Biophys. Acta Mol. Cell Biol Lipids.* 1862:513–522. https://doi.org/10.1016/j.bbalip.2017.02.002

Trovo, L., T. Ahmed, Z. Callaerts-Vegh, A. Buzzi, C. Bagni, M. Chuah, T. Vandendriessche, R. D'Hooge, D. Balschun, and C.G. Dotti. 2013. Low hippocampal PI(4,5)P(2) contributes to reduced cognition in old mice as a result of loss of MARCKS. *Nat. Neurosci.* 16:449–455. https://doi.org/10.1038/nn.3342

van den Bogaart, G., K. Meyenberg, H.J. Risselada, H. Amin, K.I. Willig, B.E. Hubrich, M. Dier, S.W. Hell, H. Grubmüller, U. Diederichsen, and R. Jahn. 2011. Membrane protein sequestering by ionic protein-lipid interactions. *Nature.* 479:552–555. https://doi.org/10.1038/nature10545

Várnai, P., and T. Balla. 1998. Visualization of phosphoinositides that bind pleckstrin homology domains: calcium- and agonist-induced dynamic changes and relationship to myo-[3H]inositol-labeled phosphoinositide pools. *J. Cell Biol.* 143:501–510. https://doi.org/10.1083/jcb.143.2.501

Várnai, P., G. Gulyás, D.J. Tóth, M. Sohn, N. Sengupta, and T. Balla. 2017. Quantifying lipid changes in various membrane compartments using lipid binding protein domains. *Cell Calcium.* 64:72–82. https://doi.org/10.1016/j.ceca.2016.12.008

Verkhratsky, A., and M. Nedergaard. 2018. Physiology of astroglia. *Physiol. Rev.* 98:239–389. https://doi.org/10.1152/physrev.00042.2016

Wenk, M.R., L. Lucast, G. Di Paolo, A.J. Romanelli, S.F. Suchy, R.L. Nussbaum, G.W. Cline, G.I. Shulman, W. McMurray, and P. De Camilli. 2003. Phosphoinositide profiling in complex lipid mixtures using electrospray

ionization mass spectrometry. *Nat. Biotechnol.* 21:813–817. https://doi.org/10.1038/nbt837

Wenk, M.R., L. Pellegrini, V.A. Klenchin, G. Di Paolo, S. Chang, L. Daniell, M. Arioka, T.F. Martin, and P. De Camilli. 2001. PIP kinase Igamma is the major PI(4,5)P(2) synthesizing enzyme at the synapse. *Neuron.* 32: 79–88. https://doi.org/10.1016/s0896-6273(01)00456-1

Willars, G.B., S.R. Nahorski, and R.A. Challiss. 1998. Differential regulation of muscarinic acetylcholine receptor-sensitive polyphosphoinositide pools and consequences for signaling in human neuroblastoma cells. *J. Biol. Chem.* 273:5037–5046. https://doi.org/10.1074/jbc.273.9.5037

Winks, J.S., S. Hughes, A.K. Filippov, L. Tatulian, F.C. Abogadie, D.A. Brown, and S.J. Marsh. 2005. Relationship between membrane phosphatidylinositol-4,5-bisphosphate and receptor-mediated inhibition of native neuronal M channels. *J. Neurosci.* 25:3400–3413. https://doi.org/10.1523/jneurosci.3231-04.2005

Xu, C., and L.M. Loew. 2003. Activation of phospholipase C increases intramembrane electric fields in N1E-115 neuroblastoma cells. *Biophys. J.* 84:4144–4156. https://doi.org/10.1016/s0006-3495(03)75139-x

Xu, C., J. Watras, and L.M. Loew. 2003. Kinetic analysis of receptor-activated phosphoinositide turnover. *J. Cell Biol.* 161:779–791. https://doi.org/10.1083/jcb.200301070

Zewe, J.P., A.M. Miller, S. Sangappa, R.C. Wills, B.D. Goulden, G.R.V. Hammond. 2020. Probing the subcellular distribution of phosphatidylinositol reveals a surprising lack at the plasma membrane. *J. Cell Biol.* 219: e201906127. https://doi.org/10.1083/jcb.201906127

Zhang, H., L.C. Craciun, T. Mirshahi, T. Rohacs, C.M. Lopes, T. Jin, and D.E. Logothetis. 2003. PIP(2) activates KCNQ channels, and its hydrolysis underlies receptor-mediated inhibition of M currents. *Neuron.* 37:963–975. https://doi.org/10.1016/s0896-6273(03)00125-9

Supplemental material

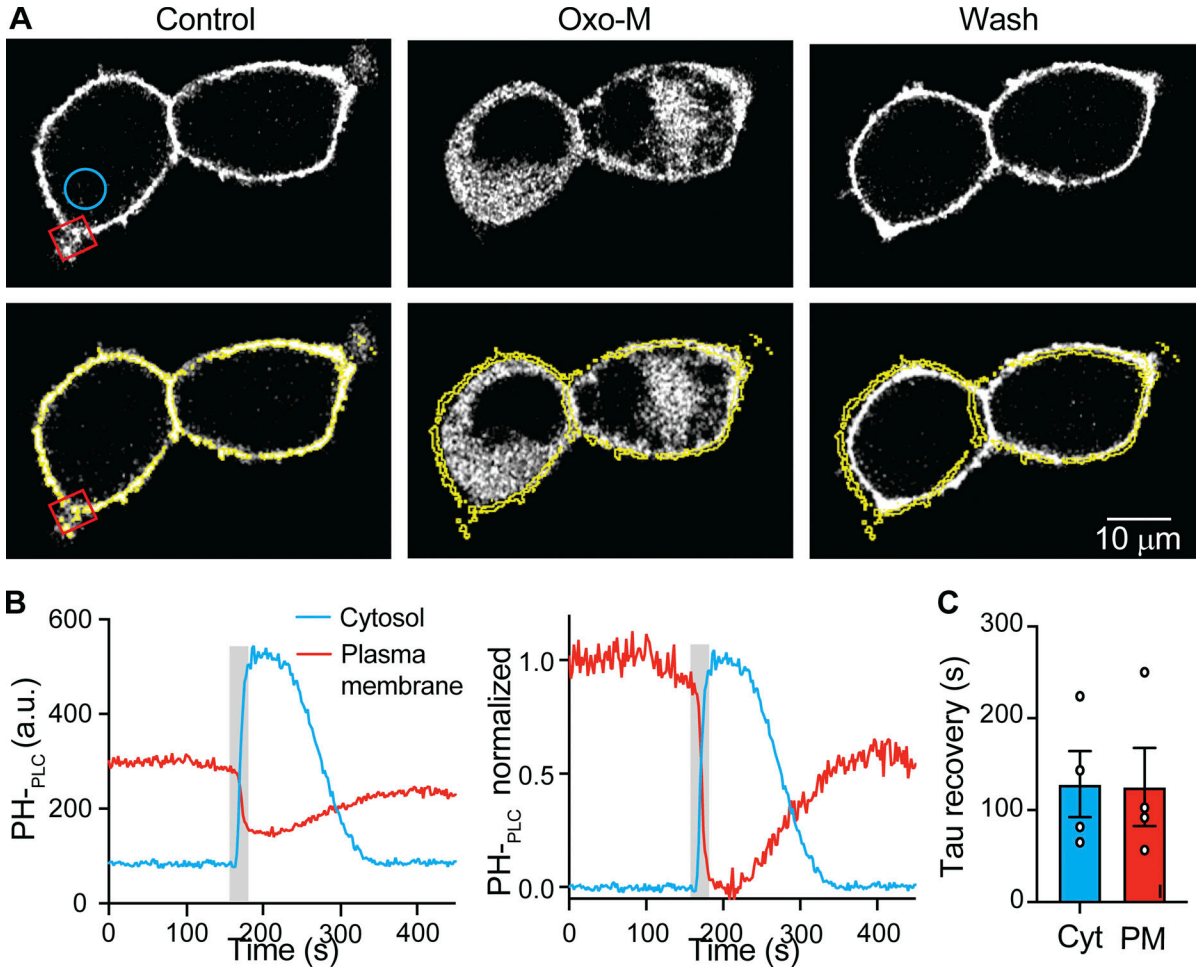

Figure S1. **Kinetics of $PH_{PLC\delta1}$ translocation measured in the cytosol is a mirror of kinetics in the PM. (A)** Representative confocal images of $PH_{PLC\delta1}$ fluorescence from M_1R-overexpressing tsA201 cells stimulated with 10 µM oxo-M. **(B)** Representative time course of cytosolic (blue circle) and PM (red square) intensity of $PH_{PLC\delta1}$ from A. The right panel shows normalized signals for better comparison. **(C)** Tau recovery after muscarinic activation measured in cytosol and PM.

Provided online is Table S1. Table S1 lists the comparison of rate constants and parameters for new hippocampal neuron and previous tsA201 cell models.